Lin et al. *Zool. Res.* 2024, 45(5): 1131−1146
https://doi.org/10.24272/j.issn.2095-8137.2024.056
https://cstr.cn/32248.14.zr.2024.056

ZR | Zoological Research

Article Open Access

Synergistic effects of Pleistocene geological and climatic events on complex phylogeographic history of widespread sympatric species of Megaloptera in East Asia

Ai-Li Lin[1,2,3,#], Ming-Ming Zou[1,#], Li-Jun Cao[4], Fumio Hayashi[5], Ding Yang[1], Xing-Yue Liu[1,*]

[1] *Department of Entomology*, *China Agricultural University*, *Beijing* 100193, *China*

[2] *Sanya Institute of China Agricultural University*, *Sanya*, *Hainan* 572025, *China*

[3] *International Joint Laboratory of Taxonomy and Systematic Evolution of Insecta*, *Henan Institute of Science and Technology*, *Xinxiang*, *Henan* 453003, *China*

[4] *Institute of Plant and Environmental Protection*, *Beijing Academy of Agriculture and Forestry Sciences*, *Beijing* 100097, *China*

[5] *Department of Biology*, *Tokyo Metropolitan University*, *Hachioji-shi*, *Tokyo* 192-0397, *Japan*

ABSTRACT

Unraveling the phylogeographic histories of species remains a key endeavor for comprehending the evolutionary processes contributing to the rich biodiversity and high endemism found in East Asia. In this study, we explored the phylogeographic patterns and demographic histories of three endemic fishfly and dobsonfly species (*Neochauliodes formosanus*, *Protohermes costalis*, and *Neoneuromus orientalis*) belonging to the holometabolan order Megaloptera. These species, which share a broad and largely overlapping distribution, were analyzed using comprehensive mitogenomic data. Our findings revealed a consistent influence of vicariance on the population isolation of *Neoc. formosanus* and *P. costalis* between Hainan, Taiwan, and the East Asian mainland during the early Pleistocene, potentially hindering subsequent colonization of the later diverged *Neon. orientalis* to these islands. Additionally, we unveiled the dual function of the major mountain ranges in East Asia, serving both as barriers and conduits, in shaping the population structure of all three species. Notably, we demonstrated that these co-distributed species originated from Southwest, Southern, and eastern Central China, respectively, then subsequently migrated along multi-directional routes, leading to their sympatric distribution on the East Asian mainland. Furthermore, our results highlighted the significance of Pleistocene land bridges along the eastern coast of East Asia in facilitating the dispersal of mountain-dwelling insects with low dispersal ability. Overall, this study provides novel insight into the synergistic impact of Pleistocene geological and climatic events in shaping the diversity and distribution of aquatic insects in East Asia.

Keywords: Comparative phylogeography; Island biogeography; Pleistocene glaciation; Corydalidae; East Asia

INTRODUCTION

Understanding the evolutionary history of the fauna and flora of East Asia is essential for comprehending the development and future fate of the region's exceptionally rich and distinctive biodiversity (Luo et al., 2023). The biogeographical history of East Asian species is shaped not only by their intrinsic adaptive capabilities, such as vagility and stress tolerance, but also by the synergistic interplay of geological and climatic factors, including Qinghai-Xizang Plateau uplift and associated orogenic events, cyclic isolation and connection of islands along the continental eastern edge of East Asia, and Quaternary glacial cycles (Du et al., 2023; Liu et al., 2023; Wei et al., 2022; Ye et al., 2016). Unlike the relatively simple "southern richness to northern purity" pattern of genetic diversity observed in European and North American species (Hewitt, 2000), East Asian species exhibit a far more complex pattern, largely attributed to the mild influence of Pleistocene glaciation and abundance of glacial refugia in low-mid latitude areas of East Asia (Fu & Wen, 2023). Thus, geological events are considered to have had a more substantial role on the phylogeographic history of East Asian species than Pleistocene climatic fluctuations (Fu & Wen, 2023; Yan et al., 2013). Recent phylogeographic studies have uncovered a variety of novel and distinctive evolutionary patterns among

Received: 02 May 2024; Accepted: 04 June 2024; Online: 05 June 2024

Foundation items: This study was supported by the National Natural Science Foundation of China (32170448, 32130012, 32300374), Beijing Natural Science Foundation (5212011), 2115 Talent Development Program of China Agricultural University, and National Animal Collection Resource Center, China

[#]Authors contributed equally to this work

*Corresponding author, E-mail: xingyue_liu@yahoo.com

the plants and animals in East Asia (Fan et al., 2012; Li et al., 2018; Qu et al., 2014; Song et al., 2018; Tang et al., 2018; Zheng et al., 2020). However, a unified understanding of these patterns and the processes that drive them remains elusive, necessitating further research and investigation (Fu & Wen, 2023).

Research on the phylogeography of East Asian insects has significantly lagged behind studies on plants and vertebrate animals, despite the extraordinary insect diversity of the region. Over the past two decades, phylogeographic patterns have been analyzed for various economically significant insects (Ji et al., 2020), agricultural and forestry pests, including major invasive species (Du et al., 2021; Ge et al., 2019; Juric et al., 2017; Ma et al., 2012; Wu et al., 2015), and neutral native insects (Tsai et al., 2021; Weng et al., 2016; Ye et al., 2018, 2020) from East Asia. A number of key phylogeographic patterns have been observed among East Asian native insects: (1) Hainan population differentiation, likely driven by isolation of the Qiongzhou Strait (Zhao et al., 2014); (2) Taiwan population differentiation, likely due to the isolation of the Taiwan Strait (Du et al., 2019; Kiyoshi, 2008; Zhu et al., 2016b); (3) Chinese and Japanese genetic exchange and differentiation, influenced by the periodic emergence and submersion of the East China Sea Land Bridge during Quaternary glaciation (Du et al., 2019; Zhang et al., 2016); (4) Korean Peninsula-Japan population differentiation, possibly resulting from the formation of the Korea/Tsushima Strait (Tojo & Itoh, 2015); (5) South-North population differentiation in mainland East Asia, possibly caused by varying climatic conditions and the barrier of the Qinling Mountains (Liu et al., 2023; Ye et al., 2020); and (6) Population differentiation in Hengduan Mountains and surrounding areas, likely driven by geographical isolation related to the uplift of the Qinghai-Xizang Plateau (Lin et al., 2022; Liu et al., 2023). Despite these advances, many important insect taxa remain unexplored in the context of East Asian phylogeography. Considering the complex interactions between geological and climatic factors in this region, there is an urgent need for additional studies, especially on the diverse native insect species.

The holometabolous insect order Megaloptera, which includes fishflies, dobsonflies, and alderflies, represents a group with significant biogeographical value due to its exclusive aquatic larval lifestyle, ancient origin, evolutionary stasis, low vagility, and disjunctive global distribution. The megalopteran fauna of East Asia exhibits an extraordinarily rich diversity, comprising over 200 species, nearly half of the global total for the order (Martins et al., 2022). Previous research into the historical biogeography of Megaloptera has revealed an *in situ* origin for the Asian Corydalidae (dobsonflies and fishflies) but a Gondwanan origin for the Asian Sialidae (alderflies), with both lineages emerging during the Cretaceous (Jiang et al., 2022). Despite the Cretaceous origin of the Asian Megaloptera, significant species diversification occurred during the Miocene, fostering the evolution of distinct endemic corydalid genera, such as *Neoneuromus* and *Parachauliodes* (Jiang et al., 2021; Yang et al., 2018). Moreover, major geological events since the Miocene, including uplift of the Himalayas and associated mountain ranges in southwestern East Asia, as well as the formation of the Japanese archipelago, Ryukyu, and Taiwan, have been identified as catalysts for speciation within the East Asian corydalids (Jiang et al., 2021; Yang et al., 2018). However, the impact of these events on the phylogeographic history and current distribution of specific Megaloptera species in East Asian remains inadequately explored. The sole study investigating the population genetics and evolutionary history of East Asian Megaloptera, specifically *Neoneuromus ignobilis* Navás, 1932, found that early vicariant events in the mountain regions of Indochina and Southwest China, followed by population expansions from South to Central and East China during the last interglacial period, likely facilitated the differentiation and broad distribution of this species (Lin et al., 2022).

Several other corydalid species in East Asia exhibit broad distributions similar to that of *Neon. ignobilis*. Among these, three species, namely *Neochauliodes formosanus* (Okamoto, 1910) (Corydalidae: Chauliodinae), *Protohermes costalis* (Walker, 1853) (Corydalidae: Corydalinae), and *Neon. orientalis* Liu & Yang, 2004 (Corydalidae: Corydalinae), show considerable overlapping distribution, often being collected from the same localities (Martins et al., 2022; Yang & Liu, 2010; Yang et al., 2018). Despite this sympatric distribution, each species exhibits some variation in its distribution boundary. *Neochauliodes formosanus* shows the broadest range, spanning all major regions of the southern Chinese mainland (Central, East, South, Southwest China), extending to northern Vietnam and many insular regions, such as Hainan, Taiwan, Tsushima Island, and Korean Peninsula. *Protohermes costalis* is endemic to China, with a range extending from the southern mainland to Taiwan, but notably absent from Hainan Island. *Neoneuromus orientalis* is restricted to the Chinese Mainland and northern Vietnam, with no insular occurrences. Notably, two lineages with distinct phenotypic and genetic divergence exist within *Neon. orientalis*, although here we consider them conspecific due to shared genital characteristics, sister-group relationship, and allopatric distribution. Despite the extensive distribution of these species, knowledge about their biology and ecology remains limited (Hayashi, 1989a, 1989b). In general, the larvae of *Neoc. formosanus* are equipped with a pair of respiratory tubes on the eighth abdominal segment, allowing them to utilize atmospheric oxygen. In contrast, the larvae of *P. costalis* and *Neon. orientalis* lack these respiratory tubes, relying more on dissolved oxygen in water. Consequently, *Neoc. formosanus* larvae may exhibit a greater adaptability to a range of freshwater habitats compared to dobsonfly larvae. Nevertheless, these three species are sometimes found co-occurring in the same stream, inhabiting similar environments without significant variation. The altitude of their habitats typically ranges from 100 to 1 500 m, based on the collection data from examined samples.

In the current study, we conducted a comparative phylogeographic analysis of three corydalid species, *Neoc. formosanus*, *P. costalis*, and *Neon. orientalis*, using mitochondrial genome (mitogenome) data. We aimed to: (1) determine whether these three sympatric species share a consistent phylogeographic history; (2) elucidate the origins of insular populations of *Neoc. formosanus* and *P. costalis* and explore the factors contributing to the absence of *Neon. orientalis* from these islands; and (3) identify the key factors driving the phylogeographic history of these megalopteran species. Overall, this study aims to provide novel insights into the evolutionary history of East Asian insects from a biogeographical perspective, shedding light on the roles that mountains and islands in East Asia have played in shaping

species distribution patterns.

MATERIALS AND METHODS

Sampling and sequencing

A comprehensive sampling effort was conducted for *Neoc. formosanus*, involving 147 specimens collected from 52 localities, spanning most of its known distribution range (Supplementary Table S1). Of these, eight specimens were dried, while all remaining specimens were preserved in 100% ethanol and stored at –20°C. For *P. costalis*, 195 specimens were sampled from 37 localities in southern China (Supplementary Table S1). Similarly, 212 specimens of *Neon. orientalis* were sampled from 29 localities in southern China and northern Vietnam (Supplementary Table S1). All voucher specimens were deposited in the Entomological Museum of China Agricultural University (CAU) in Beijing. Total genomic DNA was extracted from the thoracic muscles of each specimen using a Hipure Universal DNA Kit (Magen, China) based on the manufacturer's instructions.

To generate the mitogenomes, each sample was sequenced on the Illumina NovaSeq platform, producing 4 Gb of data using a 350 bp paired-end sequencing library. Adapter sequences from the raw reads were trimmed using Trimmomatic (Bolger et al., 2014). The *Neoc. formosanus* mitogenomes were assembled by referencing the mitogenome of a closely related species, *Neoc. rotundatus* Tjeder, 1937 (GenBank accession number: KF771894), using GENEIOUS PRIME 2020.2.4 (Kearse et al., 2012), while the *P. costalis* mitogenomes were assembled with the reference sequence of *P. costalis* (GenBank accession number: MW642321) and the *Neon. orientalis* mitogenomes were assembled in reference to the mitogenome of *Neon. ignobilis* (GenBank accession number: MT037103). The assembly parameters were configured with a minimum overlap of 25 bp, minimum overlap identity of 95%, maximum ambiguities of four, and other parameters set to default. Genetic distances among all individuals of the three species were calculated using the *COI* sequence with the Kimura 2 parameter model in MEGA v.5.0 (Tamura et al., 2011) to ensure accurate species identification.

Population genetic diversity and structure

To assess genetic diversity, the number of variable sites (*S*), haplotypes (*H*), haplotype diversity (Hd), and nucleotide diversity (π) were calculated across the different groups using the mitogenomic datasets with DNA sequence polymorphism (DNASP) v.5.0 (Librado & Rozas, 2009). Landscape shape interpolation analysis was conducted using AIS (Alleles in Space) software (Miller, 2005) based on the mitogenomic datasets to visualize the spatial patterns of genetic diversity (Manel et al., 2003; Storfer et al., 2007). The genetic distances were interpolated to produce a surface grid (50×50), with peaks and troughs reflecting regions of high and low genetic distance, respectively. Pairwise mean population differentiation (F_{ST}) was calculated using ARLEQUIN v.3.11 (Excoffier et al., 2007) based on the mitogenomic datasets.

The phylogenetic relationships among populations of the three species were reconstructed using maximum-likelihood (ML) and Bayesian inference (BI) methods based on the mitogenomic datasets. *Protochauliodes biconicus* Kimmins, 1954 (GenBank accession number: KY230493), *Chauliodes pectinicornis* (Linnaeus, 1763) (GenBank accession number: MT232273), *Nigronia serricornis* (Say, 1824) (GenBank accession number: MT232274), *Parachauliodes asahinai* Liu, Hayashi & Yang, 2008 (GenBank accession number: MT232265), and *Neoc. rotundatus* Tjeder, 1937 (GenBank accession number: OR824237) were selected as outgroup taxa for phylogenetic inference of the *Neoc. formosanus* populations. *Sialis hamata* Ross, 1937 (GenBank accession number: FJ859905), *Dysmicohermes ingens* Chandler, 1954 (GenBank accession number: KJ806318), *Nevromus exterior* Navás, 1927 (GenBank accession number: KP126232), *Protohermes concolorus* Yang & Yang, 1988 (GenBank accession number: MW642276), and *Protohermes yunnanensis* Yang & Yang, 1988 (GenBank accession number: OR823963) were selected as outgroup taxa for phylogenetic inference of the *P. costalis* populations. A similar set of outgroup taxa was used for phylogenetic inference of the *Neon. orientalis* populations, with *Neon. similis* Liu, Hayashi & Yang in Yang et al., 2018 (GenBank accession number: MW965198) replacing *P. yunnanensis*. The ML and BI analyses were performed with IQTREE (Nguyen et al., 2015) and MRBAYES v.3.2.7a implemented in the CIPRES PORTAL (Miller et al., 2009), respectively. The optimal partitioning strategy was determined by PARTITIONFINDER v.2 (Lanfear et al., 2017), with partitions divided by genes. Nodal support values for ML and BI analyses were estimated using 1 000 bootstrap replicates and Bayesian posterior probabilities, respectively.

Bayesian analysis of population structure (BAPS) v.6.0 (Cheng et al., 2013) was employed to assess spatial clustering of individuals and infer the population genetic structure for each species using the mitogenomic datasets. Split networks were generated using SPLITSTREE v.4.13.1 (Huson & Bryant, 2006) and TCS haplotype networks were constructed using Population Analysis with Reticulate Trees (POPART) (Leigh & Bryant, 2015) based on mitogenomic data. To investigate the impact of major East Asian mountains on gene flow among populations of the three corydalid species, haplotypes from different mountain populations were mapped within the haplotype network. Additionally, to visualize genetic similarities of individuals across space without biological assumptions, principal component analysis (PCA) of all samples from each species was performed using ADEGENET v.2.1.7 in the R package based on mitogenomic data.

Divergence time estimation

Divergence times among the populations of the three species were estimated using Bayesian Evolutionary Analysis by Sampling Trees (BEAST) v.2.0 (Bouckaert et al., 2014) implemented in the CIPRES PORTAL, utilizing the Yule process model and relaxed log-normal molecular clock (substitution rate of 0.0115/millions of years (Ma) for mitogenomes, including 37 genes) (Brower, 1994). Markov Chain Monte Carlo (MCMC) simulations were run with 300 million generations and sampling every 1 000 generations. TRACER v.1.7 (Rambaut et al., 2018) was used to determine stationarity and ensure that the effective sample size (ESS) of each estimated parameter was greater than 200. TREEANNOTATOR (in BEAST) was used to summarize the trees, using the "median height" option, after discarding the first 25% of samples as burn-in.

Ancestral area reconstruction

Ancestral area reconstruction was performed separately for each species to elucidate the biogeographic history underlying

population divergences. For *Neoc. formosanus*, 11 distinct regions were delineated based on population genetic structure and zoogeographical divisions of China (Zhang, 1999): A) Yunnan, B) South China, C) East of Central China, D) Southwest China, E) Hainan, F) Taiwan, G) Jiaodong Peninsula (Shandong, northern China), H) Korean Peninsula, I) Tsushima Island, J) Northern Vietnam, and K) West of Central China. For *P. costalis*, five regions were identified: B) South China, C) East of Central China, D) Southwest China, F) Taiwan, and K) West of Central China. For *Neon. orientalis*, four regions were defined: B) South China, C) East of Central China, J) Northern Vietnam, and K) West of Central China. Ancestral area reconstruction was performed using Reconstruct Ancestral State in Phylogenies (RASP) v.4.2 (build 20200103) (Yu et al., 2015), applying the optimal model estimated by the BioGeoBEARS package (Matzke, 2013). Analysis included specific distribution data for each ingroup taxon, with outgroup taxa removed. The maximum number of ancestral areas was limited to three for each species to streamline interpretation and maintain analytical tractability. Analysis utilized 8 001 post-burn-in trees for *Neoc. formosanus*, 7 229 post-burn-in trees for *P. costalis*, and 5 990 post-burn-in trees for *Neon. orientalis*, all generated from previous BEAST analyses to account for phylogenetic uncertainty.

Demographic history

To evaluate evidence of population expansion, Tajima's *D*, Fu's *F*s, and mismatch distribution analyses were performed using ARLEQUIN v.3.1.1 (Excoffier et al., 2007) and mitogenomic data. Bayesian skyline plots (BSP) implemented in BEAST v.2.0 (Bouckaert et al., 2014) were generated to detect changes in effective population size over time. The coalescent Bayesian skyline model was selected, with molecular clock and substitution rates set identically to those used for divergence time estimations. Stationarity was confirmed when ESS exceeded 200. Demographic plots were visualized using TRACER v.1.7 (Rambaut et al., 2018).

Ecological niche modeling

To compare the current suitable distribution ranges of the three species with their historical ranges, the potential and suitable distribution areas during the Last Glacial Maximum (LGM, ca. 0.022 Ma) and Last Interglacial (LIG, ca. 0.12–0.14 Ma) periods were predicted using the MAXENT module (Phillips & Dudík, 2008) in Wallace Ecological Modeling Application v.2.1.2 (Kass et al., 2023). Verified occurrence data for each species were collated (Supplementary Table S1). To reduce the effects of spatial sampling bias, a "10 km" distance threshold was applied, filtering out points that were closer to this distance than to each other. For *Neoc. formosanus*, this process removed only two locations. Climate data for the current (2.5-min resolution), LGM (2.5-min resolution), and LIG (30 arc-seconds resolution) periods were obtained from the WorldClim database (http://www.worldclim.org/; Hijmans et al., 2005). To avoid model overfitting due to the small sample size, initial climate variables were filtered according to Pearson correlation tests (Synes & Osborne, 2011), conducted using IBM SPSS v.19.0. Among each highly correlated variable pair ($|r|\geq0.85$), the one contributing more to the MAXENT model (in terms of regularized gain or percent contribution) was retained. Nine variables (bio_2 Mean Diurnal Range, bio_3 Isothermality, bio_4 Temperature Seasonality, bio_5 Max Temperature of Warmest Month, bio_6 Min Temperature of Coldest Month, bio_8 Mean Temperature of Wettest Quarter, bio_12 Annual Precipitation, bio_13 Precipitation of Wettest Month, and bio_14 Precipitation of Driest Month) were selected for analysis of *Neoc. formosanus*. Ten variables (bio_1 Annual Mean Temperature, bio_2 Mean Diurnal Range, bio_3 Isothermality, bio_5 Max Temperature of Warmest Month, bio_8 Mean Temperature of Wettest Quarter, bio_10 Mean Temperature of Warmest Quarter, bio_12 Annual Precipitation, bio_13 Precipitation of Wettest Month, bio_14 Precipitation of Driest Month, and bio_15 Precipitation Seasonality) were used for *P. costalis*. Nine variables (bio_1 Annual Mean Temperature, bio_2 Mean Diurnal Range, bio_4 Temperature Seasonality, bio_5 Max Temperature of Warmest Month, bio_8 Mean Temperature of Wettest Quarter, bio_12 Annual Precipitation, bio_14 Precipitation of Driest Month, bio_15 Precipitation Seasonality, and bio_18 Precipitation of Warmest Quarter) were used for *Neon. orientalis*. The predicted suitable zones for the three corydalid species were determined by selecting the minimum convex polygon with a 1° buffer distance.

A distribution model for the three corydalid species was constructed using MAXENT, incorporating linear, quadratic, and hinge feature classes derived from filtered occurrence records. Model performance was evaluated using area under the curve (AUC) of the receiver operating characteristic (ROC) plot, omission rate (OR), and corrected Akaike information criterion (AICc). The best model was then selected and applied to current climate data (2.5 min resolution) to infer suitable areas during the LIG and LGM periods, employing the transfer module with the threshold set to the 10-percentile training presence value. The predicted distribution maps were visualized in ARCGIS v.10.0. To compare habitat differences among the three species, bio_1 Annual Mean Temperature and bio_12 Annual Precipitation data were extracted in the current climate dataset (2.5 min resolution) according to the current distribution records of the three species and visualized using a two-dimensional (2D) map.

Isolation by distance and environment

To assess the impact of geographic distance and environmental factors on population genetic differentiation, isolation by distance (IBD) and isolation by environment (IBE) tests were conducted, respectively. IBD involved correlation analysis between geographic distances and pairwise population genetic differentiation (estimated as $F_{ST}/(1-F_{ST})$) using the Mantel test in the R package ADE4 v.1.7-22 (Dray & Dufour, 2007), with 999 permutations. Environmental distances were calculated following Cao et al. (2016) and Wang (2013). First, 19 bioclimatic variables were downloaded from the WorldClim database using the getData function in the R package RASTER (Hijmans, 2020), with bioclimatic values for each location then extracted using the cbind function. PCA was performed to analyze the 19 environmental variables for each locality using the prcomp function in R, which reduced the dimensionality of the environmental dataset. The first two principal components, which captured the most significant environmental variation across localities, were used to calculate environmental distances between locations. IBE involved correlation analysis between environmental distances and pairwise population genetic differentiation (estimated as $F_{ST}/(1–F_{ST})$) using the Mantel test in the R package ADE4 v.1.7-22, with 999 permutations.

RESULTS

Genetic structure and diversity

A total of 136 mitogenomes and 19 mitochondrial gene fragments of *Neoc. formosanus*, along with 195 mitogenomes of *P. costalis* and 212 mitogenomes of *Neon. orientalis* (NCBI GenBank accession numbers (MW642325, MW965205, PP230164, OL701282–OL701289, OL703071–OL703283, OL753214–OL753347, OM991873–OM991883, OR420135–OR420329) are shown in Supplementary Table S1), were analyzed. The genetic distances observed among the 147 samples of *Neoc. formosanus* ranged from 0% to 5.7%, while those among the 195 *P. costalis* samples ranged from 0% to 3.3% and among the 212 *Neon. orientalis* samples ranged from 0% to 6.4%, reflecting substantial genetic diversity within these populations.

The populations of *Neoc. formosanus* were divided into four groups based on BAPS analysis (Figure 1A). Group 1 included populations from Yunnan, Hainan, and some individuals from Southwest China and West of Central China. Group 2 included all samples from Taiwan. Group 3 consisted of the majority of populations from West of Central China and South China. Group 4 encompassed the remaining samples, predominantly from East of Central China, East of South China, and several insular populations from Jiaodong Peninsula, Korean Peninsula, and Tsushima Island. These groupings were corroborated by the haplotype and split networks, which also delineated four distinct groups (Figures 1F, 2D). Furthermore, the PCA results revealed a clear genetic structure and differentiation among the four groups of *Neoc. formosanus* (Figure 1D).

BAPS analysis identified four distinct groups among the *P. costalis* populations (Figure 1B). Group 1 consisted solely of samples from the Taiwan populations. Group 2 included populations from the Ta-pieh Mountains (AHMZ, HBHG, HENXX, see detail in Supplementary Table S1) and certain individuals from East of Central China. Groups 3 and 4 consisted of all remaining samples, primarily from populations in Central China, Southwest China, and South China. The haplotype and split networks (Figures 1J, 2B) confirmed the group divisions, although Group 3 in the haplotype network was divided into two parts by Groups 1 and 4 (Figure 2B). The PCA results further corroborated these findings, revealing a consistent and distinct genetic structure aligned with the BAPS results (Figure 1H).

BAPS analysis identified three distinct groups among the *Neon. orientalis* populations (Figure 1C). Group 1 included populations from Northern Vietnam and Fangchenggang (southernmost Guangxi), while all remaining samples, primarily from Central China and South China, were divided into Groups 2 and 3. The haplotype network, split network, and PCA results supported these divisions, showing a clear genetic structure and genetic differentiation among the three groups (Figures 1M, P, 2C; Supplementary Table S2).

The genetic diversity metrics for the three corydalid species, including haplotype (*H*) number, haplotype diversity (Hd), and nucleotide diversity (π), are shown in Table 1. Among the species analyzed, *Neoc. formosanus* exhibited the highest genetic diversity. Within *Neoc. formosanus*, Groups 1 and 2 showed greater genetic diversity compared to Groups 3 and 4. Conversely, within *P. costalis*, Groups 1 and 2 showed lower genetic diversity than Groups 3 and 4. For *Neon. orientalis*, genetic diversity across the three groups was relatively uniform. Landscape shape interpolation revealed a higher genetic diversity in the southwestern populations compared to the northeastern populations for both *Neoc. formosanus* and *Neon. orientalis* (Figure 1E, L). In contrast, the genetic diversity of *P. costalis* populations increased toward the eastern regions, with lower diversity observed in the western regions within their sampling range (Figure 1I).

The YN and TW (see detail in Supplementary Table S1) populations of *Neoc. formosanus* showed significantly higher genetic differentiation from the other populations (Figure 3). The TW, AHMZ, HBHG, and HENXX populations of *P. costalis* exhibited significantly higher differentiation from the other populations (Figure 3). The GXFC population of *Neon. orientalis* showed markedly higher differentiation from the other populations, with the AHHS, ZJTM, HBJG, ZJSM and FJTA populations also demonstrating significant differentiation from the other populations (Figure 3).

The haplotype distribution among the major mountain ranges of East Asia for the three corydalid species spanned several regions, including the Hengduan Mountains, easternmost edge of the Qionglai Mountains, Nanling Mountains, Wuling Mountains, Wuyi Mountains, Ta-pieh Mountains, and Tianmu Mountains. In the haplotype network (Figure 2), haplotypes from Nanling were present in all mainland groups of the three species, closely related to haplotypes from the Hengduan, Wuling, and Wuyi Mountains. Haplotypes from the Tianmu Mountains showed a close relationship with those from the Wuyi Mountains across all three species, with a close relationship with Nanling haplotypes also observed in *Neoc. formosanus* (Figure 2D). Overall, our analyses revealed a stronger haplotype connection between geographically proximate mountain ranges, such as the Hengduan and Wuling Mountains and the Nanling and Wuyi Mountains. Interestingly, despite their geographical separation, a close haplotype relationship was observed between the Hengduan and Nanling Mountains. In contrast, haplotypes from other geographically distant mountain ranges (e.g., Hengduan and Wuyi Mountains and Tianmu and Wuling Mountains) exhibited greater differentiation (Figure 2D).

Phylogenetic analysis and molecular dating

The ML and BI analyses, based on mitogenomic data, yielded consistent phylogenies for the three corydalid species. BSP analysis of divergence times (in millions of years (Ma)) revealed that *Neoc. formosanus* and its putative sister species *Neoc. rotundatus* diverged approximately 2.591 Ma (95% HPD: 1.929–3.273 Ma) (Figure 4A; Supplementary Table S3). Notably, the Hainan population emerged as the sister group to the remaining populations, with divergence during the early Pleistocene (1.992 Ma, 95% HPD: 1.488–2.523 Ma). The Taiwan population formed the sister group to all mainland populations, with divergence estimated at 1.692 Ma (95% HPD: 1.291–2.147 Ma). Further divergences were also identified within other clades. Notably, the Yunnan population diverged 1.408 Ma (95% HPD: 1.064–1.770 Ma) from its sister lineage, which included Group 3, Group 4, and some populations from Southwest and Central China (Group 1). Clade 3 diverged from its sister clade, including Groups 3 and 4, approximately 1.192 Ma (95% HPD: 0.902–1.490 Ma). The divergence between Groups 3 and 4 was dated to 0.992 Ma (95% HPD: 0.764–1.233 Ma). Within Group 4, populations from the Korean Peninsula and Tsushima Island, and a

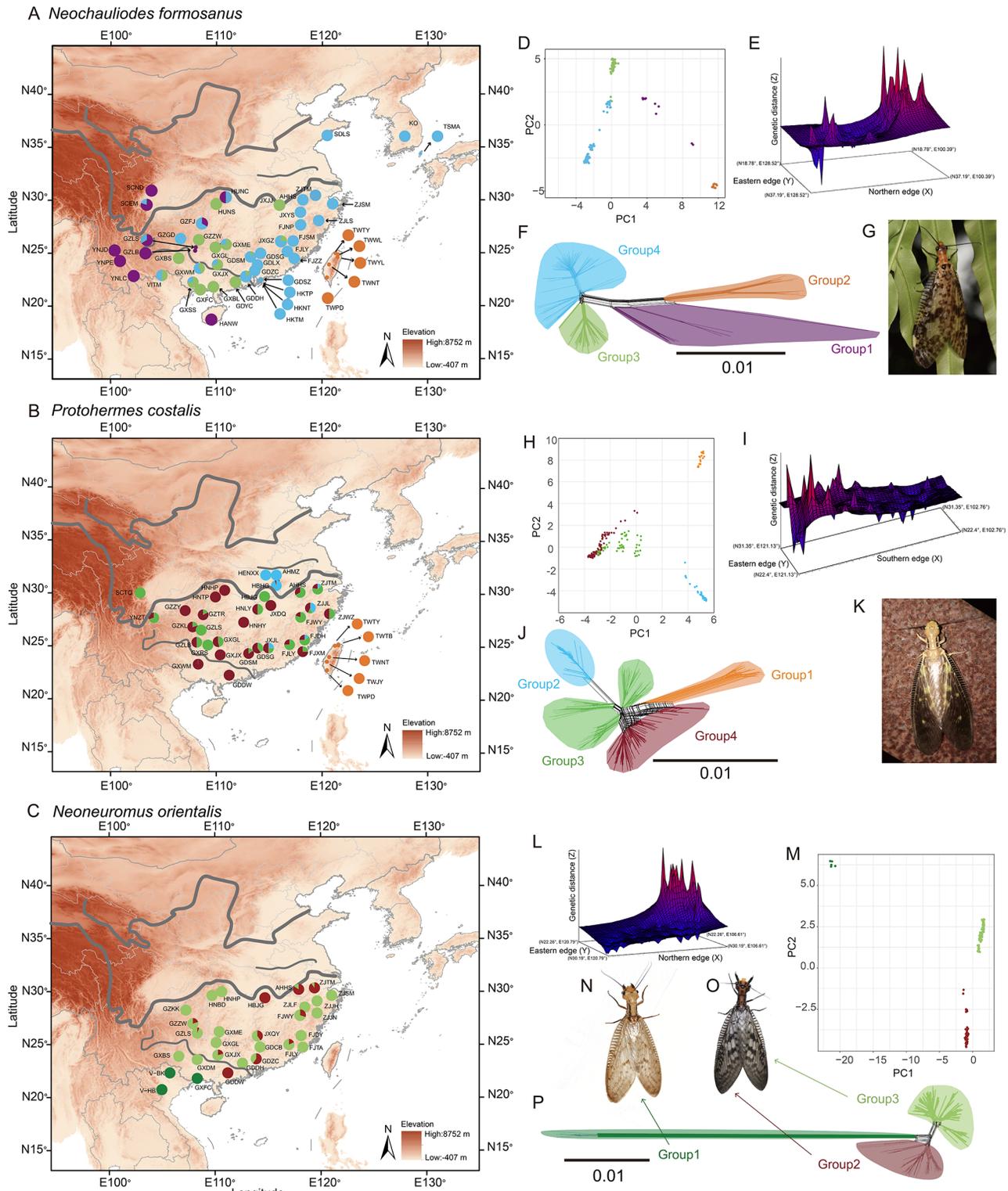

Figure 1 Population genetic structure, split tree, PCA, and landscape shape interpolation of *Neochauliodes formosanus*, *Protohermes costalis*, and *Neoneuromus orientalis*

A–C: Population genetic structure of *Neoc. formosanus* (A), *P. costalis* (B), and *Neon. orientalis* (C) inferred by BAPS v.6.0, with different colored pie charts representing different groups. D, H, M: PCA results based on mitogenomic data for *Neoc. formosanus* (D), *P. costalis* (H), and *Neon. orientalis* (M). F, J, P: Split tree of *Neoc. formosanus* (F), *P. costalis* (J), and *Neon. orientalis* (P), with different colored clades representing different groups. E, I, L: Landscape shape interpolation results for *Neoc. formosanus* (E), *P. costalis* (I), and *Neon. orientalis* (L), with X and Y axes reflecting geographic coordinates and Z axis representing genetic distances between samples. G: Adult *Neoc. formosanus* (Photo by Wei Dong). K: Adult *P. costalis* (Photo by Xing-Yue Liu). N: Adult *Neon. orientalis* in northern Vietnam (Photo by Xing-Yue Liu). O: Adult *Neon. orientalis* in Hunan, China (Photo by Xing-Yue Liu). Map of China was downloaded from the Ministry of Natural Resources (http://bzdt.ch.mnr.gov.cn/), with the map approval number GS(2020)4619.

Table 1 Genetic diversity of groups of three corydalid species based on mitogenomic data

Species	Population	No.	*S*	*H*	Hd	π
Neochauliodes formosanus	All samples	136	2 029	134	0.999	0.0110
	Group1	13	735	13	1.000	0.0165
	Group2	9	341	9	1.000	0.0091
	Group3	35	571	34	0.998	0.0047
	Group4	79	1 117	78	1.000	0.0053
Protohermes costalis	All samples	195	1 343	195	1.000	0.0086
	Group1	20	166	20	1.000	0.0028
	Group2	40	249	40	1.000	0.0020
	Group3	56	622	56	1.000	0.0063
	Group4	79	739	79	1.000	0.0046
Neoneuromus orientalis	All samples	212	1 906	184	0.998	0.0100
	Group1	5	224	5	1.000	0.0066
	Group2	78	783	68	0.996	0.0061
	Group3	129	1 032	111	0.997	0.0058

S, number of polymorphic sites; *H*, number of haplotypes; Hd, haplotype diversity; π, nucleotide diversity.

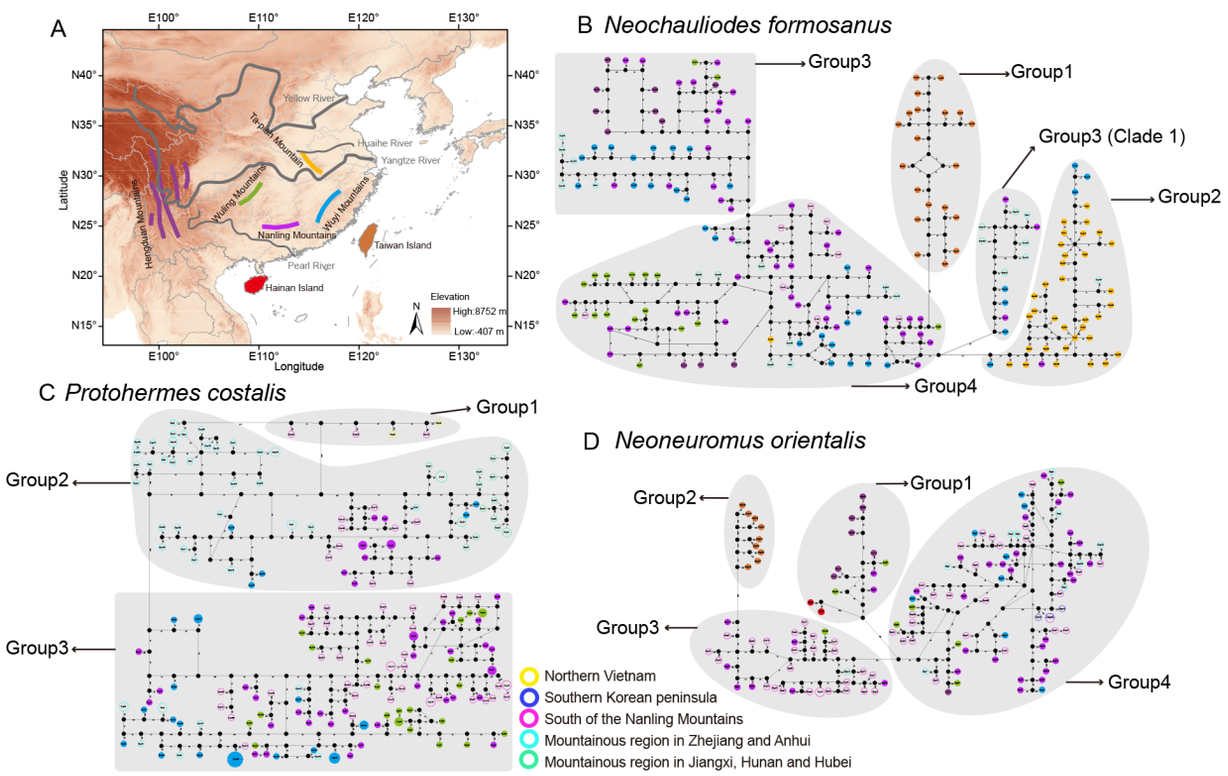

Figure 2 Haplotype network among *Neochauliodes formosanus*, *Protohermes costalis,* and *Neoneuromus orientalis* populations

A: Map of East Asia, with major mountains and islands colored to correspond with haplotype color. B: Haplotype network of *P. costalis* populations. C: Haplotype network of *Neon. orientalis* populations. D: Haplotype network of *Neoc. formosanus* populations. Specific population assignment information of mountains and islands is shown in Supplementary Table S4. Map of China was downloaded from the Ministry of Natural Resources (http://bzdt.ch.mnr.gov.cn/), with map approval number GS(2020)4619.

sample from South China, formed a monophyletic group, which diverged from a lineage containing many samples from South China and eastern Central China approximately 0.497 Ma (95% HPD: 0.366 Ma–0.628 Ma).

Protohermes costalis and its putative sister species *P. yunnanensis* diverged approximately 2.049 Ma (95% HPD: 1.568–2.547 Ma) (Figure 4B; Supplementary Table S3). Group 1 (Taiwan populations) was identified as the sister group to the remaining populations, with divergence estimated at 1.677 Ma (95% HPD: 1.300–2.065 Ma). The divergence between Group 2 and its sister clade, including Groups 3 and 4, was estimated at 1.462 Ma (95% HPD: 1.148–1.814 Ma). Within Clade 3, Groups 3 and 4 diverged approximately 1.110 Ma (95% HPD: 0.859–1.377 Ma).

Neoneuromus orientalis and its putative sister species *Neon. similis* diverged approximately 1.535 Ma (95% HPD: 1.219–1.864 Ma) (Figure 4C; Supplementary Table S3). Group 1 (populations from Northern Vietnam and Fangchenggang in Guangxi, China) initially diverged from its sister group, including all remaining populations, approximately 1.371 Ma (95% HPD: 1.107–1.673 Ma). The GDDW population in Group 2 diverged from its sister clade, which included Group 3 and the other Group 2 clade, occurred about 1.111 Ma (95% HPD: 0.891–1.343 Ma). Group 3

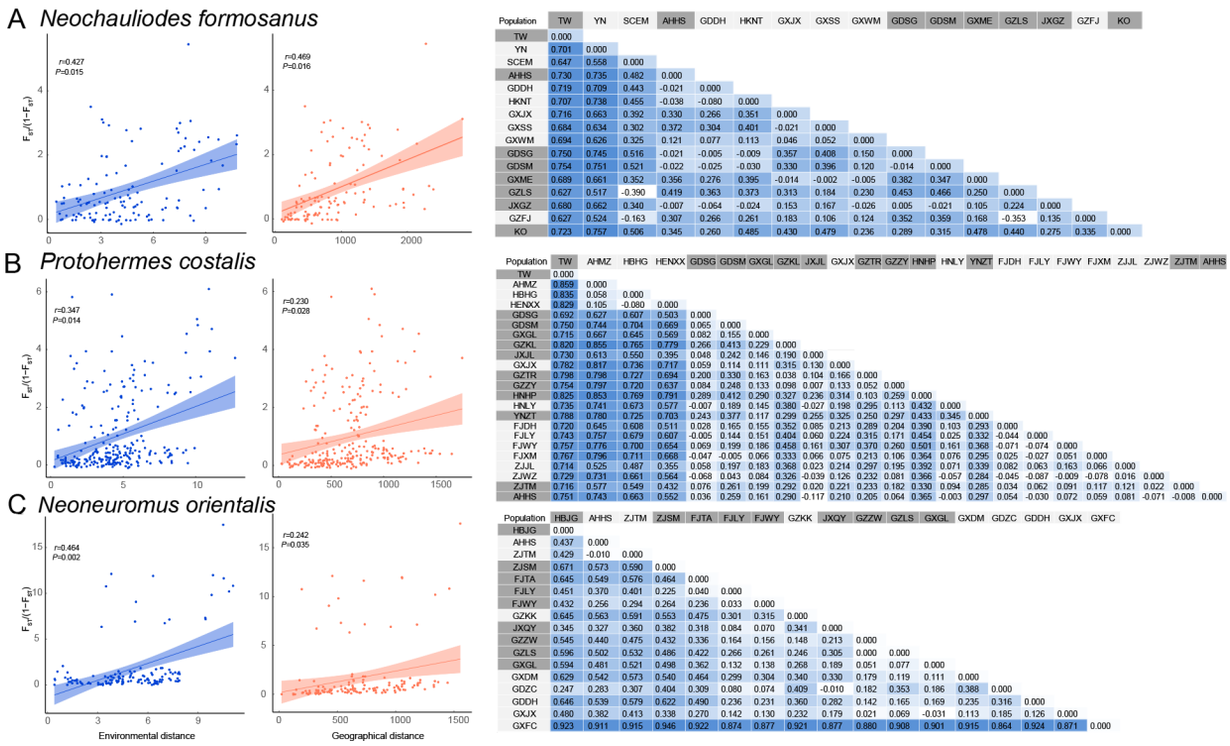

Population	TW	YN	SCEM	AHHS	GDDH	HKNT	GXJX	GXSS	GXWM	GDSG	GDSM	GXME	GZLS	JXGZ	GZFJ	KO
TW	0.000															
YN	0.701	0.000														
SCEM	0.647	0.558	0.000													
AHHS	0.730	0.735	0.482	0.000												
GDDH	0.719	0.709	0.443	-0.021	0.000											
HKNT	0.707	0.738	0.455	-0.038	-0.080	0.000										
GXJX	0.716	0.663	0.392	0.330	0.266	0.351	0.000									
GXSS	0.684	0.634	0.302	0.372	0.304	0.401	-0.021	0.000								
GXWM	0.694	0.626	0.325	0.121	0.077	0.113	0.046	0.052	0.000							
GDSG	0.750	0.745	0.516	-0.021	-0.005	-0.009	0.357	0.408	0.150	0.000						
GDSM	0.754	0.751	0.521	-0.022	-0.025	-0.030	0.330	0.396	0.120	-0.014	0.000					
GXME	0.689	0.661	0.352	0.356	0.276	0.395	-0.014	-0.002	-0.005	0.382	0.347	0.000				
GZLS	0.627	0.517	-0.390	0.419	0.363	0.373	0.313	0.184	0.230	0.453	0.466	0.250	0.000			
JXGZ	0.680	0.662	0.340	-0.007	-0.064	-0.024	0.153	0.167	-0.026	0.005	-0.021	0.105	0.224	0.000		
GZFJ	0.627	0.524	-0.163	0.307	0.266	0.261	0.183	0.106	0.124	0.352	0.359	0.168	-0.353	0.135	0.000	
KO	0.723	0.757	0.506	0.345	0.260	0.485	0.430	0.479	0.236	0.289	0.315	0.478	0.440	0.275	0.335	0.000

Population	TW	AHMZ	HBHG	HENXX	GDSG	GDSM	GXGL	GZKL	JXJL	GXJX	GZTR	GZZY	HNHP	HNLY	YNZT	FJDH	FJLY	FJWY	FJXM	ZJJL	ZJWZ	ZJTM	AHHS
TW	0.000																						
AHMZ	0.859	0.000																					
HBHG	0.835	0.058	0.000																				
HENXX	0.829	0.105	-0.080	0.000																			
GDSG	0.692	0.627	0.607	0.503	0.000																		
GDSM	0.750	0.744	0.704	0.669	0.065	0.000																	
GXGL	0.715	0.667	0.645	0.569	0.082	0.155	0.000																
GZKL	0.820	0.855	0.765	0.779	0.266	0.413	0.229	0.000															
JXJL	0.730	0.613	0.550	0.395	0.048	0.242	0.146	0.190	0.000														
GXJX	0.782	0.817	0.736	0.717	0.059	0.114	0.111	0.315	0.130	0.000													
GZTR	0.798	0.798	0.727	0.694	0.200	0.330	0.163	0.038	0.104	0.166	0.000												
GZZY	0.754	0.797	0.720	0.637	0.084	0.248	0.133	0.098	0.007	0.133	0.052	0.000											
HNHP	0.825	0.853	0.769	0.791	0.289	0.412	0.290	0.327	0.236	0.314	0.103	0.259	0.000										
HNLY	0.735	0.741	0.673	0.577	-0.007	0.189	0.145	0.380	-0.027	0.198	0.296	0.113	0.432	0.000									
YNZT	0.788	0.780	0.725	0.703	0.243	0.377	0.117	0.299	0.255	0.325	0.250	0.297	0.433	0.345	0.000								
FJDH	0.720	0.645	0.608	0.511	0.028	0.165	0.155	0.352	0.085	0.213	0.289	0.204	0.390	0.103	0.293	0.000							
FJLY	0.743	0.757	0.679	0.607	-0.005	0.144	0.151	0.404	0.060	0.224	0.315	0.171	0.454	0.025	0.332	-0.044	0.000						
FJWY	0.757	0.776	0.700	0.654	0.069	0.199	0.196	0.458	0.161	0.307	0.370	0.260	0.501	0.161	0.368	-0.071	-0.074	0.000					
FJXM	0.767	0.796	0.711	0.668	-0.047	-0.005	0.066	0.333	0.066	0.075	0.213	0.106	0.364	0.076	0.295	0.025	-0.027	0.051	0.000				
ZJJL	0.714	0.525	0.487	0.355	0.058	0.197	0.183	0.368	0.023	0.214	0.297	0.195	0.392	0.071	0.339	0.082	0.063	0.163	0.066	0.000			
ZJWZ	0.729	0.731	0.661	0.564	-0.068	0.043	0.084	0.326	-0.039	0.126	0.232	0.081	0.366	-0.057	0.284	-0.045	-0.087	-0.009	-0.078	0.016	0.000		
ZJTM	0.716	0.577	0.549	0.432	0.076	0.261	0.199	0.292	0.020	0.221	0.233	0.182	0.330	0.094	0.285	0.034	0.062	0.091	0.117	0.121	0.022	0.000	
AHHS	0.751	0.743	0.663	0.552	0.036	0.259	0.161	0.290	-0.117	0.210	0.205	0.064	0.365	-0.003	0.297	0.054	-0.030	0.072	0.059	0.081	-0.071	-0.008	0.000

Population	HBJG	AHHS	ZJTM	ZJSM	FJTA	FJLY	FJWY	GZKK	JXQY	GZZW	GZLS	GXGL	GXDM	GDZC	GDDH	GXJX	GXFC
HBJG	0.000																
AHHS	0.437	0.000															
ZJTM	0.429	-0.010	0.000														
ZJSM	0.671	0.573	0.590	0.000													
FJTA	0.645	0.549	0.576	0.464	0.000												
FJLY	0.451	0.370	0.401	0.225	0.040	0.000											
FJWY	0.432	0.256	0.294	0.264	0.236	0.033	0.000										
GZKK	0.645	0.563	0.591	0.553	0.475	0.301	0.315	0.000									
JXQY	0.345	0.327	0.360	0.382	0.318	0.084	0.070	0.341	0.000								
GZZW	0.545	0.440	0.475	0.432	0.336	0.164	0.156	0.148	0.213	0.000							
GZLS	0.596	0.502	0.532	0.486	0.422	0.266	0.261	0.246	0.305	0.000	0.000						
GXGL	0.594	0.481	0.521	0.498	0.362	0.132	0.138	0.268	0.189	0.051	0.077	0.000					
GXDM	0.629	0.542	0.573	0.540	0.464	0.299	0.304	0.340	0.330	0.179	0.119	0.111	0.000				
GDZC	0.247	0.283	0.307	0.404	0.309	0.080	0.074	0.409	-0.010	0.182	0.353	0.186	0.388	0.000			
GDDH	0.646	0.539	0.579	0.622	0.490	0.236	0.231	0.360	0.282	0.142	0.165	0.169	0.235	0.316	0.000		
GXJX	0.480	0.382	0.413	0.338	0.270	0.142	0.130	0.232	0.179	0.021	0.069	-0.031	0.113	0.185	0.126	0.000	
GXFC	0.923	0.911	0.915	0.946	0.922	0.874	0.877	0.921	0.877	0.880	0.908	0.901	0.915	0.864	0.924	0.871	0.000

Figure 3 IBE (left), IBD (middle), and F_{ST} (right) analyses for *Neochauliodes formosanus* (A), *Protohermes costalis* (B), and *Neoneuromus orientalis* (C)

Alternating gray and white population background colors represent different mountain/island populations. Specific population assignment information of mountains and islands is shown in Supplementary Table S4. Intensity of blue represents size of F_{ST} value between pairs of populations, dark blue represents high F_{ST} value, light blue represents low F_{ST} value.

diverged from Group 2, except for the GDDW population, approximately 1.000 Ma (95% HPD: 0.812–1.201 Ma).

Ancestral area reconstruction

The best models estimated by the standard statistical model selection for *Neoc. formosanus*, *P. costalis*, and *Neon. orientalis* were DIV+j, DIVALIKE+j, and DIV+j, respectively. The ancestral range of all *Neoc. formosanus* populations included Yunnan, Hainan, and Taiwan (Figure 4A). Yunnan and Taiwan were reconstructed as the ancestral range of most populations, except the Hainan population. The divergence of the Hainan and Taiwan populations from the mainland populations was attributed to vicariance events (Figure 4A: Nodes 2, 3). Yunnan was reconstructed as the ancestral range of the mainland populations as well as those from the Korean Peninsula and Tsushima Island (Figure 4A: Node 4). South China was reconstructed as the ancestral range of Group 3+Group 4, as well as for the individual groups. Several major dispersal events were inferred from the analysis (Figure 4D). The first event likely involved an early dispersal from Yunnan to South China and western Central China (Figure 4A: Node 4). The second event suggested multiple dispersals from South China to Central China (Figure 4A: Node 5). The third event indicated westward dispersal from western Central China to neighboring Southwest China (Figure 4A: Node 10). Additionally, the populations from the Jiaodong Peninsula, Korean Peninsula, and Tsushima Island were inferred to have originated from dispersal events out of South China (Supplementary Figure S1).

The ancestral range of all populations of *P. costalis* included Taiwan and eastern Central China (Figure 4B; Supplementary Figure S2). A vicariance event likely occurred between the Taiwan (Group 1) and mainland populations (Figure 4B: Node 2). Eastern Central China was reconstructed as the ancestral range of all mainland populations (Figure 4B: Node 3), including Group 2 and Group 3+Group 4. South China was inferred as the ancestral range of the lineage including Group 4 and the two clades of Group 3 (Figure 4B: Node 5). Western Central China was inferred as the ancestral range of the lineage including Group 4 and one clade of Group 3. Among the major divergences of Groups 2, 3, and 4, several early dispersals were inferred, including movements from eastern Central China to South China and from South China to western Central China. Subsequently, a large number of multidirectional dispersals were detected among these areas (Figure 4D).

The ancestral range of all populations of *Neon. orientalis* comprised South China and Northern Vietnam (Figure 4C; Supplementary Figure S3). A vicariance event was inferred between Group 1 (populations of Northern Vietnam and southernmost Guangxi) and Group 2+Group 3 (Figure 4C: Node 2). South China was reconstructed as the ancestral range of Group 2+Group 3, as well as that of Groups 2 and 3, respectively (Figure 4C: Nodes 3, 8). Northward dispersals were inferred from South China to Central China (Figure 4D).

Demographic history analysis

Tajima's *D* and mismatch distribution analyses indicated that all three corydalid species may have undergone population expansions (Supplementary Figure S4). BSP analysis suggested that *Neoc. formosanus* underwent one fast expansion during 0.14–0.10 Ma, *P. costalis* underwent a long-term population expansion during 0.45–0.02 Ma (Figure 5), and *Neon. orientalis* underwent two population expansions

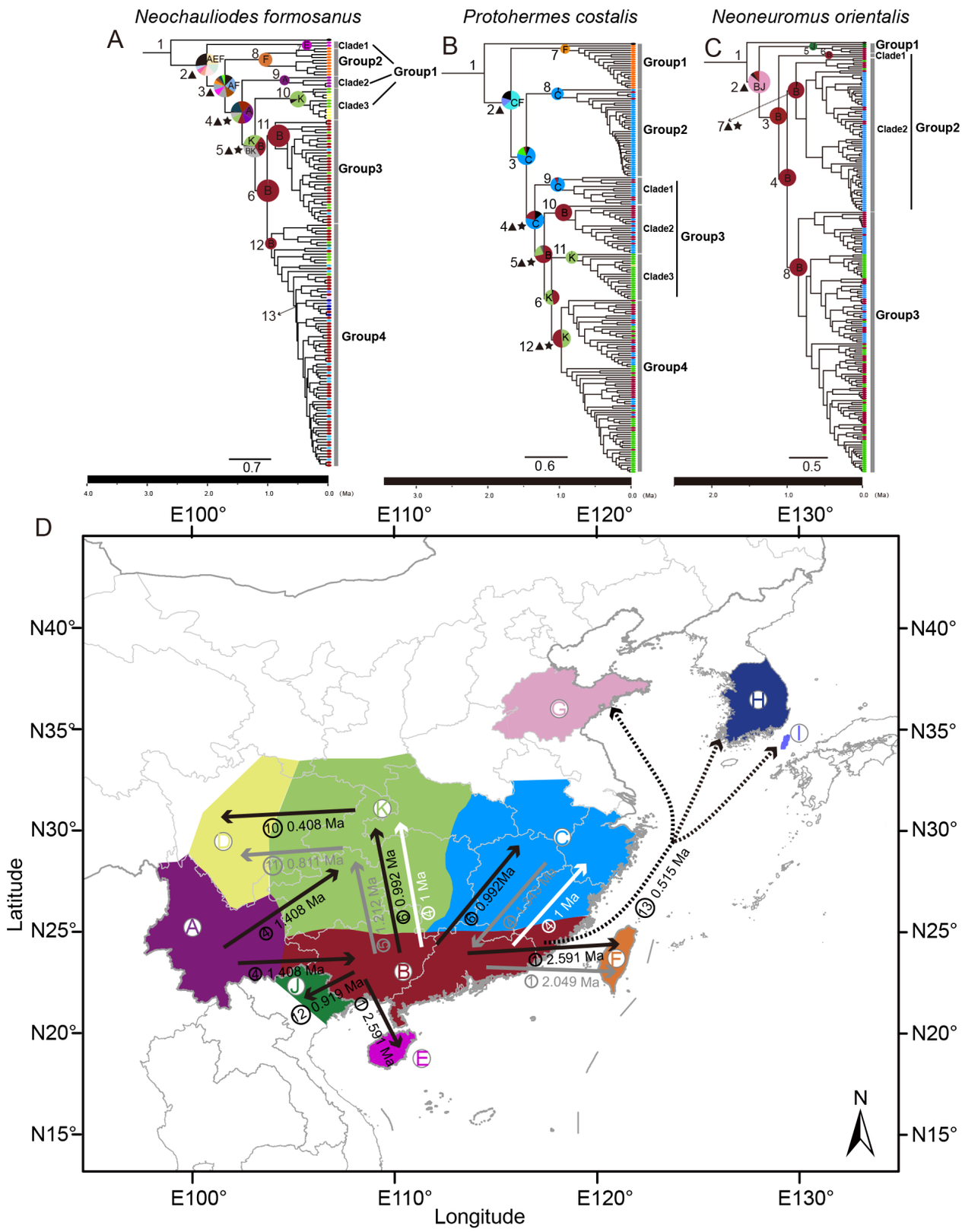

Figure 4 Spatial and temporal divergence among *Neochauliodes formosanus*, *Protohermes costalis*, and *Neoneuromus orientalis* populations

A: Chronogram of *Neoc. formosanus*. B: Chronogram of *P. costalis*. C: Chronogram of *Neon. orientalis*. D: Map of East Asia, with colored areas of endemism for ancestral area reconstruction, and dispersal routes of each species. Node divergence times are provided in Supplementary Table S3. Pentacles represent dispersal events and triangles represent vicariance events. Black arrows indicate dispersal path of *Neoc. formosanus*, gray arrows indicate dispersal path of *P. costalis*, and white arrows indicate dispersal path of *Neon. orientalis*. Node numbers in the chronogram are shown in circles adjacent to the arrows, with estimated dispersal times provided aside corresponding arrows. Map of China was downloaded from the Ministry of Natural Resources (http://bzdt.ch.mnr.gov.cn/), with map approval number GS (2020) 4619.

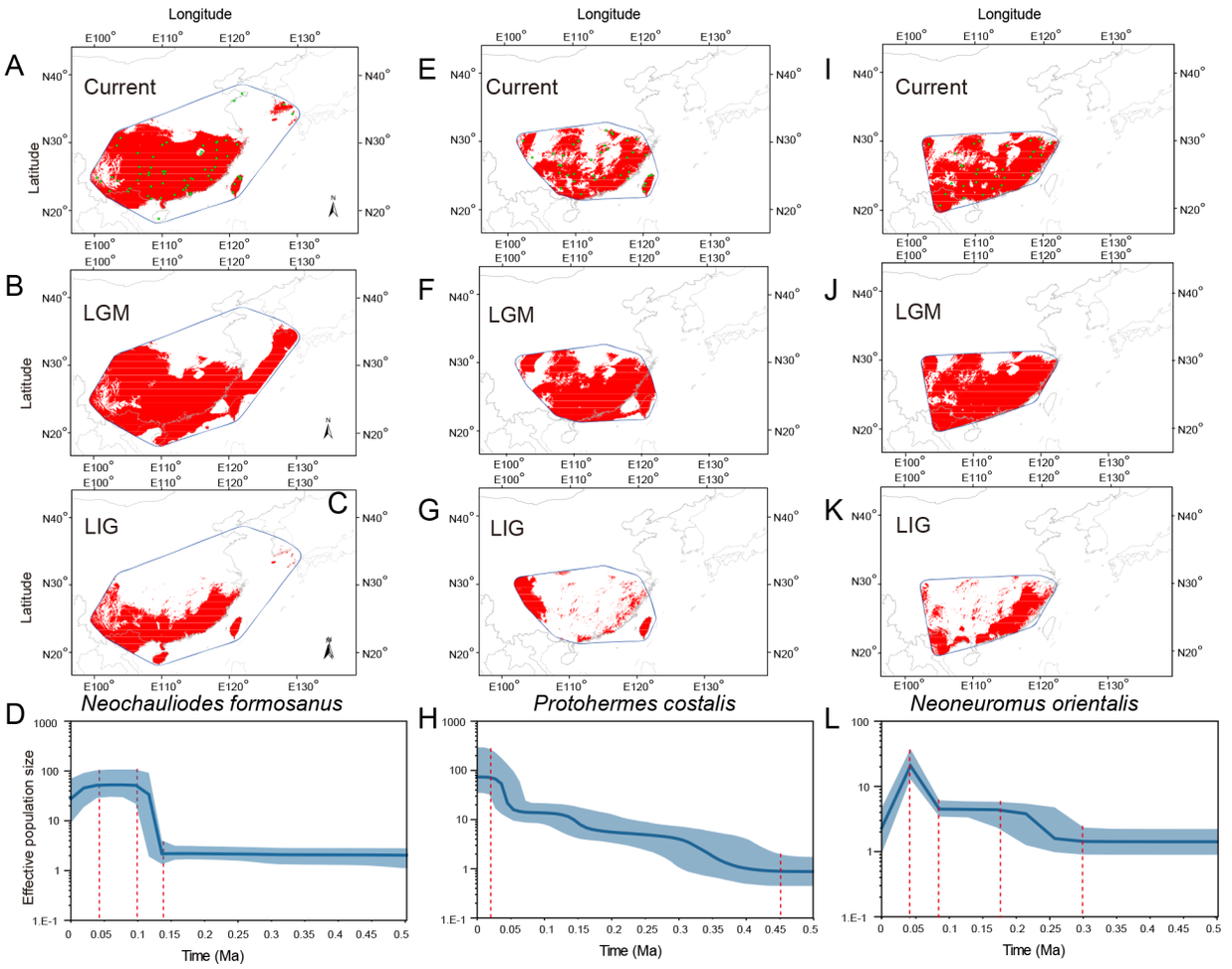

Figure 5 Ecological niche modeling under 10-percentile training presence threshold and Bayesian skyline plots (BSP) for *Neochauliodes formosanus* (A–D), *Protohermes costalis* (E–H), and *Neoneuromus orientalis* (I–L) during current, last glacial maximum (LGM), and last interglacial (LIG) periods

Green dots represent localities with known records used for fitting ecological niche model. In BSP analyses, estimates of means are joined by solid lines, while shaded area represents 95% high posterior density (HPD) limits. Map of China was downloaded from the Ministry of Natural Resources (http://bzdt.ch.mnr.gov.cn/), with map approval number GS(2020)4619.

during 0.30–0.18 Ma and 0.07–0.04 Ma, respectively (Figure 5). However, both *Neon. orientalis* and *Neoc. formosanus* experienced population shrinkage from the end of the Pleistocene (ca. 0.04 Ma) to the Holocene (Figure 5). To determine the potential causes of population shrinkage and specific geographic distributions, historical dynamic analysis should be performed for each geographic population. However, due to uneven sampling and low sample sizes in some geographic populations, the populations of the two species were divided into multiple groups for analysis based on genetic structure, geographical flora, mountain information, and other factors (Supplementary Figure S5). Results indicated that the *Neoc. formosanus* populations experienced significant shrinkage, particularly in the Hengduan Mountains and adjacent areas (i.e., northern Vietnam and southwestern Guangxi). In contrast, the *Neon. orientalis* populations in the Nanling Mountains and areas south of Nanling Mountains did not exhibit shrinkage (Supplementary Figure S5).

Ecological niche modeling

Ecological niche modeling for *Neoc. formosanus* (best model LQ_2.5: auc.val.avg=0.715, or.10p.avg=0.131, delta.AICc=0), *P. costalis* (best model H3: auc.val.avg=0.724, or.10p.avg=0.103, delta.AICc=0), and *Neon. orientalis* (best model H2: auc.val.avg=0.72, or.10p.avg=0.161, delta.AICc=0) indicated strong predictive performance. The predictions for current suitable distributions for the three corydalid species were similar to their actual sample distributions (Figure 5). The LGM distributions for the three species showed similar ranges to their current suitable distribution areas, with land bridges connecting the mainland to Hainan Island, Taiwan Island, Korean Peninsula, and Tsushima Island for *Neoc. formosanus* and *P. costalis*. However, when projecting these niches into LIG climate conditions, the models indicated that large areas of Central China would have been unsuitable for these species (Figure 5).

Ecological niche modeling also revealed that bio_12 Annual Precipitation was the main factor affecting the suitable habitat range for all three species. The response curves for bio_12 Annual Precipitation in the best-fit models—LQ_2.5 for *Neoc. formosanus*, H3 for *P. costalis*, and H2 for *Neon. orientalis*—indicated that habitat suitability remained stable under conditions of higher annual precipitation. However, when annual precipitation fell below 160 mm (represented as 1 600 mm on the x-axis due to WorldClim scaling), suitability for *Neon. orientalis* and *P. costalis* decreased sharply, and when annual precipitation fell below 250 mm, suitability for

Neoc. formosanus decreased sharply (Supplementary Figure S6A–C). 2D ecological visualization based on bio_1 Annual Mean Temperature and bio_12 Annual Precipitation suggested that *Neoc. formosanus* may have a greater tolerance to a wider temperature and precipitation range compared to the other two species (Supplementary Figure S6D).

Isolation by distance and environment

The Mantel tests for IBD and IBE revealed significant correlations for all three corydalid species (Figure 3). Notably, IBE analysis demonstrated a highly significant correlation for *Neon. orientalis* (r=0.464, P=0.002) compared to the other two species. In contrast, IBD analysis showed similar significant correlations across all three species (Figure 3).

DISCUSSION

Origin of insular populations

Our results showed that the Taiwan populations of *Neoc. formosanus* and *P. costalis* were genetically distinct from their mainland counterparts, diverging during the late Pliocene and early Pleistocene. Similarly, although the Hainan population of *Neoc. formosanus* was grouped with the Yunnan populations in BAPS analysis, it was found to be genetically independent, with its isolation dated slightly earlier than that of the Taiwan populations. This early divergence between mainland and insular populations highlights the significant role of island isolation in shaping the genetic endemism of insular populations in Corydalidae. The observed genetic endemism of the Hainan and Taiwan populations may also be related to the low vagility of these species. In contrast, species with stronger dispersal capabilities, such as the East Asian birds *Alcippe morrisonia* and *Stachyridopsis ruficeps* (Qu et al., 2015), widespread bat *Hipposideros armiger* (Lin et al., 2014), and oriental garden lizard *Calotes versicolor* (Huang et al., 2013), appear to experience more frequent gene flow between Hainan, Taiwan and the East Asian mainland.

Our haplotype network and ancestral area reconstruction analyses clearly indicated that the Hainan and Taiwan populations originated from colonization by their mainland ancestors. The ancestral ranges, which include regions of South China and eastern Central China, along with the close haplotype relationships between these mainland populations and the Taiwan population, suggest that these areas likely served as the source for the Taiwan population. Geological and faunal analyses support this inference, indicating that Taiwan was connected to the Asian continent by a land bridge during the Pliocene (Huang et al., 1995; Ota, 1991, 1997; Yu, 1995). Nevertheless, the timing of dispersal events between the mainland and Taiwan differed slightly between the two corydalid species. The insular colonization of *Neoc. formosanus* potentially occurred approximately 0.5 million years earlier than that of *P. costalis*. Notably, the divergence between the mainland and Taiwan populations of *Neoc. formosanus* (1.692 Ma (95% HPD: 1.291–2.147 Ma)) and *P. costalis* (1.677 Ma (95% HPD: 1.300–2.065 Ma)) appear to have been synchronous, likely driven by the same vicariance event, possibly isolation of the island isolation or submersion of the land bridge during the early Pleistocene, leading to population differentiation. This hypothesis is further supported by the vicariance events identified in the ancestral area reconstruction (Figure 4A: Node 3, Figure 4B: Node 2), which emphasize the role of island isolation in driving the differentiation of these insular populations.

The inferred mainland origin of the Hainan population of *Neoc. formosanus* was located around Southwestern China, as suggested by the close haplotype relationships observed between the populations from Hainan, Yunnan, Guizhou, and Sichuan. The southeastward dispersal into Hainan may have followed a route through South China (e.g., Guangxi) or Northern Vietnam, given the probable existence of a land connection between Hainan and the mainland at the Beibu Gulf (Liang, 2013; Replumaz & Tapponnier, 2003; Wan, 2011; Zhang et al., 2005) and the remarkable biotic similarities between Hainan and Vietnam (Jiang et al., 2019; Zhu, 2016, 2017). Although the Hainan and Yunnan populations were both classified into Group 1, the genetic distance between the Hainan and mainland populations, including those in Yunnan, ranged from 0.034 to 0.055. The estimated divergence time of the Hainan population (1.992 Ma (95% HPD: 1.488–2.523 Ma)) generally aligns with the separation of Hainan from the mainland due to the emergence of the Qiongzhou Strait, driven by rising sea levels during the early Pleistocene (c. 2 Ma) (Zhao et al., 2007; Zhu et al., 2016a).

In contrast to the early isolation of the Hainan and Taiwan populations, the insular *Neoc. formosanus* population from Tsushima Island and the nearby population from the Korean Peninsula exhibited low genetic endemism but significant admixture with populations from South China and eastern Central China. Similarly, the *Neoc. formosanus* population from Jiaodong Peninsula was genetically closer to those from Tsushima and South China. Phylogeographic analysis suggested that these northeastern insular and peninsular populations likely originated in South China and migrated northward along a corridor provided by the East China Sea land bridges during the middle and late Pleistocene, a period when these regions would have been highly suitable for the species distribution (Figure 5). Similar dispersal patterns have been proposed for other species, such as the assassin bug *Sphedanolestes impressicollis*, Indo-Malayan *Polyura* butterfly species group, rock shell *Thais clavigera*, and amphipod *Amphiareus obscuriceps*, all of which exhibit close genetic relationships among populations from the southeastern Chinese Mainland, Korean peninsula, and Japanese archipelago (Du et al., 2019; Guo et al., 2015; Toussaint & Balke, 2016; Ye et al., 2014; Zhang et al., 2016). These studies support the idea that Pleistocene land bridges facilitated the dispersal of insects inhabiting lowland and coastal regions. However, such dispersal is not expected for insects inhabiting highland regions or those with poor dispersal abilities (Tojo et al., 2017). Therefore, the successful dispersal of *Neoc. formosanus* to the Korean Peninsula and Tsushima Island is particularly remarkable, given the mountain-dwelling habit and low vagility of fishflies.

Another notable issue arises from the absence of *Neon. orientalis* on any of the East Asian islands. Our molecular dating indicated that the divergence of *Neon. orientalis* from its sister species (1.535 Ma (95% HPD: 1.219–1.864 Ma)) occurred much later in than that of *Neoc. formosanus* (2.591 Ma (95% HPD: 1.929–3.273Ma)) and *P. costalis* (2.049 Ma (95% HPD: 1.568–2.547 Ma)), both of which have populations established on Hainan and Taiwan. Crucially, the divergence of *Neon. orientalis* also occurred later than that of the Hainan and mainland populations (1.992 Ma (95% HPD: 1.488–2.523 Ma)) of *Neoc. formosanus* and the Taiwan and mainland

populations of *Neoc. formosanus* (1.692 Ma (95% HPD: 1.291–2.147 Ma)) and *P. costalis* (1.677 Ma (95% HPD: 1.300–2.065 Ma)). Despite the presence of land bridges between these islands and the East Asian mainland during Pleistocene glaciations, no subsequent insular colonization could be traced in these corydalid species, suggesting that Hainan and Taiwan have served as significant barriers to corydalid dispersal since the late Pleistocene. The later divergence of *Neon. orientalis* likely meant it missed the window of opportunity for migration to these islands. A similar explanation may account for the absence of insular populations in the widespread species *Neon. ignobilis* (closely related to *Neon. orientalis*), which likely diverged contemporaneously with *Neon. orientalis* (Lin et al., 2022).

Role of mountains: Barrier or corridor

Mountains play a crucial role as both barriers and corridors, significantly shaping the phylogeographic patterns of species (Muellner-Riehl, 2019; Smissen et al., 2013; Wang et al., 2022). Here, Mantel tests revealed a strong positive correlation between genetic differentiation and geographical distance among the three corydalid species, highlighting their limited dispersal abilities and heightened sensitivity to geographical isolation. These findings underscore the influence of major mountain ranges as barriers to population differentiation in these species across in the East Asian mainland. For instance, the Hengduan Mountains, which formed alongside the uplift of the Qinghai-Xizang Plateau, likely facilitated divergence of the Yunnan populations of *Neoc. formosanus* during the Pleistocene (1.692 Ma, 95% HPD: 1.291–2.147 Ma). A similar barrier effect of this mountain range has been observed in the dobsonfly species *Neon. ignobilis* (Lin et al., 2022). In East China, the Ta-pieh Mountains, located at the junction of Anhui, Hubei, and Henan, may have acted as a barrier that isolated Group 2 of *P. costalis* (including the HENXX, AHMZ, and HBHG populations) from other mainland populations during the Pleistocene (1.462 Ma, 95% HPD: 1.148–1.814 Ma). Additionally, the Shiwandashan Mountains, situated at the border of China and Vietnam, likely contributed to the early divergence of Group 1 of *Neon. orientalis* (comprising populations from Northern Vietnam and Fangchenggang in Guangxi) around 1.371 Ma (95% HPD: 1.107–1.673 Ma).

While mountains often act as barriers, they also function as corridors for the dispersal of species, as illustrated in our haplotype network (Figure 2). The Nanling Mountain range, in particular, appears to be an important diffusion corridor for the three corydalid species. Spanning more than 1 000 km from west to east, this range forms a natural boundary between Guangxi-Guangdong and Hunan-Jiangxi, connecting the Yunnan-Guizhou Plateau in the west and Wuyi Mountains in the east. The Nanling Mountains also represent a significant ecological divide in subtropical China, distinguishing mid- and northern subtropical climates from southern subtropical or tropical climates. Long considered a major glacial refugium, this region harbors high biodiversity in East Asia (Huang et al., 2012; Qiu et al., 2011; Tian et al., 2018; Xu et al., 2021). Previous research on various East Asian plants (e.g., *Eomecon chionantha* and *Sargentodoxa cuneata*) has shown that the Nanling Mountains act as an essential corridor for species dispersal (Qiu et al., 2011; Tian et al., 2015, 2018; Yang et al., 2019). The geographic location and favorable climatic condition of the Nanling Mountains likely facilitate their role as a dispersal corridor for the East Asian corydalid species. Despite the limited flight ability of adult corydalids, their larvae, which inhabit lotic streams and rivers, may disperse over considerable distances to other mountainous areas with similar freshwater habitats. However, this dispersal does not appear to follow major rivers (e.g., Yangtze River), as evidenced by the absence of close genetic relationships among populations near these rivers. Furthermore, the haplotype network revealed gene flow among adjacent mountain populations (e.g., Wuyi Mountains vs. Tianmu Mountains, Wuyi Mountains vs. Ta-pieh Mountains, northern Hengduan Mountains vs. Wuling Mountains), highlighting the roles of East Asian mountains as corridors for corydalid dispersal. The geological impact on the phylogeographic history of these species likely extend to other aquatic insects with similar ecological niches and biology, warranting further investigation.

Sympatric distribution with complex phylogeographic patterns

Our comparative phylogeographic analyses provide crucial insights into the evolutionary history of the three sympatric corydalid species from the East Asian mainland. The distribution of *Neoc. formosanus* across the mainland likely originated from eastward dispersal, first from Yunnan to South China and West of Central China. This was followed by northeastward dispersal from South China to East of Central China, and northwestward dispersal from South China through West of Central China to Southwest China. In contrast, the mainland populations of *P. costalis* likely originated in northeastern areas, specifically East of Central China, followed by southwestward dispersal to South China and subsequent dispersal through West of Central China to Southwest China. For *Neon. orientalis*, dispersal events appear to have occurred from South China toward both East and West of Central China, mirroring the phylogeographic history of the congeneric species *Neon. ignobilis* (Lin et al., 2022). These migration processes are believed to have occurred during the Pleistocene glacial cycles, starting around 3 Ma. The broad and overlapping distributions of these species across South, Central, and Southwest China were likely established prior to the LGM. The existence of multiple refugia in the Hengduan Mountains and South China suggests that the dispersal routes observed in *Neoc. formosanus* and *Neon. orientalis*, from south to north, west to east, or southwest to northeast, represent a broader pattern of dispersal seen in numerous East Asian species (Fan et al., 2011; Li et al., 2018; Qu et al., 2014, 2015; Wei & Zhang, 2022; Ye et al., 2016). Nevertheless, the southwestward dispersal from East of Central China, as observed in *P. costalis*, is relatively rare (Fu & Wen, 2023), highlighting the significant role of the Ta-pieh Mountains and nearby ranges (e.g., Tianmu Mountains) as refugia in eastern China.

Post-glaciation expansion patterns in East Asian species are species-specific and vary in timing, direction, and scale due to the relatively weak impact of the Pleistocene glaciation (Fu & Wen, 2023). Demographic histories also varied among the three studied species in the context of the entire population assembly. Notably, *P. costalis* exhibited a long-term population expansion between 0.02–0.45 Ma (Figure 5), while *Neoc. formosanus* and *Neon. orientalis* experienced population contractions from the Late Pleistocene to Holocene (ca. 0–0.04 Ma) after the LIG expansion. Ecological niche

modeling revealed an expansion in the suitable habitat area for all three species from the LIG to LGM. However, when comparing the demographic history of different *Neoc. formosanus* groups, only the Hengduan Mountain populations underwent contraction (Supplementary Figure S5), which may be due to the unfavorable habitats in the Hengduan Mountains (Figure 5) and the low gene flow among populations in this region. In contrast, *Neon. orientalis* populations in the Nanling Mountains did not experience contraction from the end of Pleistocene to the Holocene (Supplementary Figure S5). The Nanling Mountains, which were never glaciated, maintained stable environmental conditions during the last glacial period, including consistent annual precipitation (an important factor for the suitable distribution of *Neon. orientalis*) (Xiao et al., 2007). These stable conditions likely contributed to the persistence of *Neon. orientalis* populations in this region. Additionally, interspecific competition with the closely related and usually sympatric congener *Neon. ignobilis* may have contributed to the population shrinkage of *Neon. orientalis*, alongside climatic factors. The timing of population expansions in these two species is also consistent (Lin et al., 2022). However, while *Neon. ignobilis* experienced continued population expansion into the Holocene, achieving a broader distribution range extending from southern Indochina to the Qinling Mountains, *Neon. orientalis* populations began contracting at the end of Pleistocene, with their range limited to South and Central China, extending only as far south as northern Indochina (Yang et al., 2018). This suggests that interspecific competition for ecological resources may have driven the different phylogeographic histories of these two species.

Among the three corydalid species studied, *Neoc. formosanus* has the broadest range and is the only one extending into the Palearctic region. Notably, *Neoc. formosanus* appears to have migrated northward to the Korean peninsula and Tsushima Island via Pleistocene land bridges, despite ecological niche modeling suggesting that these land connections along the eastern coast of East Asia were suitable for all three corydalid species. The population expansion of *Neoc. formosanus* may be attributed to its stronger adaptability to a diverse range of habitats (Supplementary Figure S6). A key factor contributing to this adaptability is the presence of respiratory tubes on the eighth abdominal segment of fishfly larvae, including *Neoc. formosanus*—a feature in all dobsonfly larvae. These tubes allow fishfly larvae to access atmospheric oxygen and thrive in various lentic freshwater habitats with low dissolved oxygen, including slow-flowing streams, shallow stream edges, and ponds (Hayashi, 1989c; Smith, 1970). This biological trait likely facilitated the expansion of *Neoc. formosanus* into a greater variety of habitats under Pleistocene environmental change.

CONCLUSIONS

This study represents the first comparative phylogeographic analysis of the aquatic insect order Megaloptera, highlighting species-specific phylogeographic histories among the three East Asian corydalid species studied. Although these species share largely overlapping mainland distributions, the processes of population differentiation and expansion differed across species. A key finding was the consistent impact of early Pleistocene isolation between populations on Hainan, Taiwan, and the East Asian mainland. Additionally, our research elucidated the dual role of major mountain ranges in East Asia, acting as both barriers and corridors in shaping the population structure of East Asian corydalids. Our results also provided evidence for the significance of Pleistocene land bridges along the eastern coast of East Asia in facilitating the dispersal of insects inhabiting, including those inhabiting lowlands, coastal regions, and mountainous areas with low dispersal abilities. Overall, this study offers new insights into the historical dynamics of species in East Asia under Pleistocene glacial cycling, and sheds light on the island biogeography of aquatic insects. Future research should extend these analyses to more widely distributed megalopteran species in East Asia and other regions, using whole-genome-scale data to further elucidate the historical and ecological factors shaping phylogeographic patterns.

SUPPLEMENTARY DATA

Supplementary data to this article can be found online.

COMPETING INTERESTS

The authors declare that they have no competing interests.

AUTHORS' CONTRIBUTIONS

A.L.L.: Sample collection, Data curation, Formal analysis, Investigation, Methodology, Software, Writing – original draft, Writing – review & editing. M.M.Z.: Sample collection, Data curation, Formal analysis, Writing – review & editing. L.J.C.: Methodology, Software, Writing – review & editing. F.H.: Sample collection, Investigation, Writing – review and editing. D.Y.: Sample collection, Investigation, Writing – review and editing. X.Y.L.: Conceptualization, Data curation, Funding acquisition, Project administration, Investigation, Methodology, Writing – original draft, Writing – review & editing. All authors read and approved the final version of the manuscript.

ACKNOWLEDGMENTS

We are grateful to the collectors of all specimens studied herein, with particular thanks to Dr. Minh Lan Pham (Plant Quarantine Subdepartment No. 8, Lao Cai) for kind help during the collecting trips in Vietnam with official permission. We also thank the three anonymous referees who critically read and improved the manuscript.

REFERENCES

Bolger AM, Lohse M, Usadel B. 2014. Trimmomatic: a flexible trimmer for Illumina sequence data. *Bioinformatics*, **30**(15): 2114–2120.

Bouckaert R, Heled J, Kühnert D, et al. 2014. BEAST 2: a software platform for Bayesian evolutionary analysis. *PLoS Computational Biology*, **10**(4): e1003537.

Brower AV. 1994. Rapid morphological radiation and convergence among races of the butterfly *Heliconius erato* inferred from patterns of mitochondrial DNA evolution. *Proceedings of the National Academy of Sciences of the United States of America*, **91**(14): 6491–6495.

Cao LJ, Li ZM, Wang ZH, et al. 2016. Bulk development and stringent selection of microsatellite markers in the western flower thrips *Frankliniella occidentalis*. *Scientific Reports*, **6**: 26512.

Cheng L, Connor TR, Sirén J, et al. 2013. Hierarchical and spatially explicit clustering of DNA sequences with BAPS software. *Molecular Biology and Evolution*, **30**(5): 1224–1228.

Dray S, Dufour AB. 2007. The ade4 package: implementing the duality diagram for ecologists. *Journal of Statistical Software*, **22**(4): 1–20.

Du ZY, Ishikawa T, Liu H, et al. 2019. Phylogeography of the assassin bug *Sphedanolestes impressicollis* in East Asia inferred from mitochondrial and nuclear gene sequences. *International Journal of Molecular Sciences*, **20**(5): 1234.

Du ZY, Wu YF, Chen Z, et al. 2021. Global phylogeography and invasion history of the spotted lanternfly revealed by mitochondrial phylogenomics. *Evolutionary Applications*, **14**(4): 915–930.

Du ZY, Zhao Q, Wang X, et al. 2023. Climatic oscillation promoted diversification of spinous assassin bugs during Pleistocene glaciation. *Evolutionary Applications*, **16**(4): 880–894.

Excoffier L, Laval G, Schneider S. 2007. Arlequin (version 3.0): an integrated software package for population genetics data analysis. *Evolutionary Bioinformatics Online*, **1**: 47–50.

Fan ZX, Liu SY, Liu Y, et al. 2011. How quaternary geologic and climatic events in the southeastern margin of the Tibetan Plateau influence the genetic structure of small mammals: inferences from phylogeography of two rodents, *Neodon irene* and *Apodemus latronum. Genetica*, **139**(2): 339–351.

Fan ZX, Liu SY, Liu Y, et al. 2012. Phylogeography of the south China field mouse (*Apodemus draco*) on the southeastern Tibetan Plateau reveals high genetic diversity and glacial refugia. *PLoS One*, **7**(5): e38184.

Fu JZ, Wen LY. 2023. Impacts of Quaternary glaciation, geological history and geography on animal species history in continental East Asia: a phylogeographic review. *Molecular Ecology*, **32**(16): 4497–4514.

Ge XZ, He SY, Zhu CY, et al. 2019. Projecting the current and future potential global distribution of *Hyphantria cunea* (Lepidoptera: Arctiidae) using CLIMEX. *Pest Management Science*, **75**(1): 160–169.

Guo X, Zhao D, Jung D, et al. 2015. Correction: phylogeography of the rock shell *Thais clavigera* (mollusca): evidence for long-distance dispersal in the northwestern pacific. *PLoS One*, **10**(8): e0135540.

Hayashi F. 1989a. Life history of *Protohermes costalis* (Walker) in Taiwan. *Nature and Insects*, **24**: 25–27.

Hayashi F. 1989b. *Neochauliodes sinensis* (Walker) in Taiwan. *Konchu to Shizen*, **24**(9): 28–31.

Hayashi F. 1989c. Microhabitat selection by the fishfly larva, *Parachauliodes japonicus*, in relation to its mode of respiration. *Freshwater Biology*, **21**(3): 489–496.

Hewitt G. 2000. The genetic legacy of the Quaternary ice ages. *Nature*, **405**(6789): 907–913.

Hijmans RJ. 2020. Raster: geographic data analysis and modeling. https://CRAN.R-project.org/package=raster.

Hijmans RJ, Cameron SE, Parra JL, et al. 2005. Very high resolution interpolated climate surfaces for global land areas. *International Journal of Climatology*, **25**(15): 1965–1978.

Huang CY, Yuan PB, Song SR, et al. 1995. Tectonics of short–lived intra–arc basins in the arc–continent collision terrane of the Coastal Range, eastern Taiwan. *Tectonics*, **14**(1): 19–38.

Huang JH, Chen B, Liu CR, et al. 2012. Identifying hotspots of endemic woody seed plant diversity in China. *Diversity and Distributions*, **18**(7): 673–688.

Huang Y, Guo XG, Ho SYW, et al. 2013. Diversification and demography of the oriental garden lizard (*Calotes versicolor*) on Hainan island and the adjacent mainland. *PLoS One*, **8**(6): e64754.

Huson DH, Bryant D. 2006. Application of phylogenetic networks in evolutionary studies. *Molecular Biology and Evolution*, **23**(2): 254–267.

Ji YK, Li XG, Ji T, et al. 2020. Gene reuse facilitates rapid radiation and independent adaptation to diverse habitats in the Asian honeybee. *Science Advances*, **6**(51): eabd3590.

Jiang XL, Gardner EM, Meng HH, et al. 2019. Land bridges in the Pleistocene contributed to flora assembly on the continental islands of South China: insights from the evolutionary history of *Quercus championii*. *Molecular Phylogenetics and Evolution*, **132**: 36–45.

Jiang YL, Yang F, Yue L, et al. 2021. Origin and spatio-temporal diversification of a fishfly lineage endemic to the islands of East Asia (Megaloptera: Corydalidae). *Systematic Entomology*, **46**(1): 124–139.

Jiang YL, Yue L, Yang F, et al. 2022. Similar pattern, different paths: tracing the biogeographical history of Megaloptera (Insecta: Neuropterida) using mitochondrial phylogenomics. *Cladistics*, **38**(3): 374–391.

Juric I, Salzburger W, Balmer O. 2017. Spread and global population structure of the diamondback moth *Plutella xylostella* (Lepidoptera: Plutellidae) and its larval parasitoids *Diadegma semiclausum* and *Diadegma fenestrale* (Hymenoptera: Ichneumonidae) based on mtDNA. *Bulletin of Entomological Research*, **107**(2): 155–164.

Kass JM, Pinilla-Buitrago GE, Paz A, et al. 2023. *Wallace* 2: a shiny app for modeling species niches and distributions redesigned to facilitate expansion via module contributions. *Ecography*, **2023**(3): e06547.

Kearse M, Moir R, Wilson A, et al. 2012. Geneious Basic: an integrated and extendable desktop software platform for the organization and analysis of sequence data. *Bioinformatics*, **28**(12): 1647–1649.

Kiyoshi T. 2008. Differentiation of golden-ringed dragonfly *Anotogaster sieboldii* (Selys, 1854) (Cordulegastridae: Odonata) in the insular East Asia revealed by the mitochondrial gene genealogy with taxonomic implications. *Journal of Zoological Systematics and Evolutionary Research*, **46**(2): 105–109.

Lanfear R, Frandsen PB, Wright AM, et al. 2017. PartitionFinder 2: new methods for selecting partitioned models of evolution for molecular and morphological phylogenetic analyses. *Molecular Biology and Evolution*, **34**(3): 772–773.

Leigh JW, Bryant D. 2015. POPART: full-feature software for haplotype network construction. *Methods in Ecology and Evolution*, **6**(9): 1110–1116.

Li J, Wei S, Hu M, et al. 2018. Reflection of paleoclimate oscillations and tectonic events in the phylogeography of moustache toads in southern China. *Journal of Zoology*, **305**(1): 17–26.

Liang GH. 2013. Eight evidences about Hainan Island separated from Chinas Beibuwan Gulf with drifting and rotation. *Acta Geologica Sinica*, **87**: 73–76.

Librado P, Rozas J. 2009. DnaSP v5: a software for comprehensive analysis of DNA polymorphism data. *Bioinformatics*, **25**(11): 1451–1452.

Lin AL, Cao LJ, Wei SJ, et al. 2022. Phylogeography of the Oriental dobsonfly, *Neoneuromus ignobilis* Navás, suggests Pleistocene allopatric isolation and glacial dispersal shaping its wide distribution. *Systematic Entomology*, **47**(1): 65–81.

Lin AQ, Csorba G, Li LF, et al. 2014. Phylogeography of *Hipposideros armiger* (Chiroptera: Hipposideridae) in the Oriental Region: the contribution of multiple Pleistocene glacial refugia and intrinsic factors to contemporary population genetic structure. *Journal of Biogeography*, **41**(2): 317–327.

Liu YX, Bu YF, Wang JL, et al. 2023. Geological events and climate change drive diversification and speciation of mute cicadas in eastern continental Asia. *Molecular Phylogenetics and Evolution*, **184**: 107809.

Luo D, Song MS, Xu B, et al. 2023. A clue to the evolutionary history of modern East Asian flora: insights from phylogeography and diterpenoid alkaloid distribution pattern of the *Spiraea japonica* complex. *Molecular Phylogenetics and Evolution*, **184**: 107772.

Ma C, Yang PC, Jiang F, et al. 2012. Mitochondrial genomes reveal the global phylogeography and dispersal routes of the migratory locust. *Molecular Ecology*, **21**(17): 4344–4358.

Manel S, Schwartz MK, Luikart G, et al. 2003. Landscape genetics: combining landscape ecology and population genetics. *Trends in Ecology & Evolution*, **18**(4): 189–197.

Martins CC, Ardila-Camacho A, Rivera-Gasperín SL, et al. 2022. A world checklist of extant and extinct species of Megaloptera (Insecta: Neuropterida). *European Journal of Taxonomy*, **812**(1): 1–93.

Matzke NJ. 2013. Probabilistic historical biogeography: new models for founder-event speciation, imperfect detection, and fossils allow improved accuracy and model-testing. *Frontiers of Biogeography*, **5**(4): 242–248.

Miller MA, Holder MT, Vos R, et al. 2009. The CIPRES Portals. CIPRES.

http://www.phylo.org/sub_sections/portal.

Miller MP. 2005. Alleles in space (AIS): computer software for the joint analysis of interindividual spatial and genetic information. *Journal of Heredity*, **96**(6): 722–724.

Muellner-Riehl AN. 2019. Mountains as evolutionary arenas: patterns, emerging approaches, paradigm shifts, and their implications for plant phylogeographic research in the Tibeto-Himalayan region. *Frontiers in Plant Science*, **10**: 195.

Nguyen LT, Schmidt HA, von Haeseler A, et al. 2015. IQ-TREE: a fast and effective stochastic algorithm for estimating maximum-likelihood phylogenies. *Molecular Biology and Evolution*, **32**(1): 268–274.

Ota H. 1991. Systematics and biogeography of terrestrial reptiles of Taiwan. In Proceedings of the First International Symposium on Wildlife Conservation, ROC (Lin, Y. S. & Chang, K. H. , eds), pp. 47–112. Taipei: Council of Agriculture.

Ota H. 1997. Historical biogeographical implications in the variation and diversity of amphibians and reptiles in Taiwan. In Proceedings of the Symposium on the Phylogeny, Biogeography and Conservation of Fauna and Flora of East Asian Region (Kue K. Y. , Chen T. H. , eds), pp. 75–86. Taipei: National Science Council, ROC

Phillips SJ, Dudík M. 2008. Modeling of species distributions with Maxent: new extensions and a comprehensive evaluation. *Ecography*, **31**(2): 161–175.

Qiu YX, Fu CX, Comes HP. 2011. Plant molecular phylogeography in China and adjacent regions: tracing the genetic imprints of Quaternary climate and environmental change in the world's most diverse temperate flora. *Molecular Phylogenetics and Evolution*, **59**(1): 225–244.

Qu YH, Ericson PGP, Quan Q, et al. 2014. Long-term isolation and stability explain high genetic diversity in the eastern Himalaya. *Molecular Ecology*, **23**(3): 807–720.

Qu YH, Song G, Gao B, et al. 2015. The influence of geological events on the endemism of East Asian birds studied through comparative phylogeography. *Journal of Biogeography*, **42**(1): 179–192.

Rambaut A, Drummond AJ, Xie D, et al. 2018. Posterior summarization in Bayesian phylogenetics using Tracer 1.7. *Systematic Biology*, **67**(5): 901–904.

Replumaz A, Tapponnier P. 2003. Reconstruction of the deformed collision zone between India and Asia by backward motion of lithospheric blocks. *Journal of Geophysical Research: Solid Earth*, **108**(B6): 2285.

Smissen PJ, Melville J, Sumner J, et al. 2013. Mountain barriers and river conduits: phylogeographical structure in a large, mobile lizard (Varanidae: *Varanus varius*) from eastern Australia. *Journal of Biogeography*, **40**(9): 1729–1740.

Smith EL. 1970. Biology and structure of the dobsonfly, *Neohermes californicus* (Walker) (Megaloptera: Corydalidae). *The Pan-Pacific Entomologist*, **46**: 142–150.

Song W, Cao LJ, Li BY, et al. 2018. Multiple refugia from penultimate glaciations in East Asia demonstrated by phylogeography and ecological modelling of an insect pest. *BMC Evolutionary Biology*, **18**(1): 152.

Storfer A, Murphy MA, Evans JS, et al. 2007. Putting the 'landscape' in landscape genetics. *Heredity*, **98**(3): 128–142.

Synes NW, Osborne PE. 2011. Choice of predictor variables as a source of uncertainty in continental-scale species distribution modelling under climate change. *Global Ecology and Biogeography*, **20**(6): 904–914.

Tamura K, Peterson D, Peterson N, et al. 2011. MEGA5: molecular evolutionary genetics analysis using maximum likelihood, evolutionary distance, and maximum parsimony methods. *Molecular Biology and Evolution*, **28**(10): 2731–2739.

Tang CQ, Matsui T, Ohashi H, et al. 2018. Author correction: identifying long-term stable refugia for relict plant species in East Asia. *Nature Communications*, **9**(1): 5241.

Tian S, Kou YX, Zhang ZR, et al. 2018. Phylogeography of *Eomecon chionantha* in subtropical China: the dual roles of the Nanling Mountains as a glacial refugium and a dispersal corridor. *BMC Evolutionary Biology*, **18**(1): 20.

Tian S, Lei SQ, Hu W, et al. 2015. Repeated range expansions and inter-/postglacial recolonization routes of *Sargentodoxa cuneata* (Oliv.) Rehd. et Wils. (Lardizabalaceae) in subtropical China revealed by chloroplast phylogeography. *Molecular Phylogenetics and Evolution*, **85**: 238–246.

Tojo K, Itoh T. 2015. Geohistory of Japan and establishment of insect fauna. *In*: Oba H, Osawa S, Insect DNA Society. Marvelous World of Insects Clarified from their Genes. Tokyo: Yushokan, 105–155.

Tojo K, Sekiné K, Takenaka M, et al. 2017. Species diversity of insects in Japan: their origins and diversification processes. *Entomological Science*, **20**(1): 357–381.

Toussaint EFA, Balke M. 2016. Historical biogeography of *Polyura* butterflies in the oriental Palaeotropics: trans-archipelagic routes and South Pacific island hopping. *Journal of Biogeography*, **43**(8): 1560–1572.

Tsai CL, Kubota K, Pham HT, et al. 2021. Ancestral haplotype retention and population expansion determine the complicated population genetic structure of the hilly lineage of *Neolucanus swinhoei* complex (Coleoptera, Lucanidae) on the subtropical Taiwan island. *Insects*, **12**(3): 227.

Wan TF. 2011. Geotectonics of China. Beijing: Geology Press, 1–501. (in Chinese)

Wang CR, Zhou TY, Qin YZ, et al. 2022. Wuling mountains function as a corridor for woody plant species exchange between northern and southern central China. *Frontiers in Ecology and Evolution*, **10**: 837738.

Wang IJ. 2013. Examining the full effects of landscape heterogeneity on spatial genetic variation: a multiple matrix regression approach for quantifying geographic and ecological isolation. *Evolution*, **67**(12): 3403–3411.

Wei SC, Sun S, Dou HL, et al. 2022. Influence of Pleistocene climate fluctuations on the demographic history and distribution of the critically endangered Chinese pangolin (*Manis pentadactyla*). *BMC Zoology*, **7**(1): 50.

Wei XP, Zhang XC. 2022. Phylogeography of the widespread fern *Lemmaphyllum* in East Asia: species differentiation and population dynamics in response to change in climate and geography. *Journal of Systematics and Evolution*, **60**(2): 411–432.

Weng YM, Yang MM, Yeh WB. 2016. A comparative phylogeographic study reveals discordant evolutionary histories of alpine ground beetles (Coleoptera, Carabidae). *Ecology and Evolution*, **6**(7): 2061–2073.

Wu YK, Molongoski JJ, Winograd DF, et al. 2015. Genetic structure, admixture and invasion success in a Holarctic defoliator, the gypsy moth (*Lymantria dispar*, Lepidoptera: Erebidae). *Molecular Ecology*, **24**(6): 1275–1291.

Xiao JY, Lü HB, Zhou WJ, et al. 2007. Evolution of vegetation and climate since the last glacial maximum recorded at Dahu peat site, South China. *Science in China Series D: Earth Sciences*, **50**(8): 1209–1217.

Xu MZ, Yang LH, Kong HH, et al. 2021. Congruent spatial patterns of species richness and phylogenetic diversity in karst flora: case study of *Primulina* (gesneriaceae). *Journal of Systematics and Evolution*, **59**(2): 251–261.

Yan F, Zhou WW, Zhao HT, et al. 2013. Geological events play a larger role than Pleistocene climatic fluctuations in driving the genetic structure of *Quasipaa boulengeri* (Anura: Dicroglossidae). *Molecular Ecology*, **22**(4): 1120–1133.

Yang AH, Zhong YD, Liu SJ, et al. 2019. New insight into the phylogeographic pattern of *Liriodendron chinense* (Magnoliaceae) revealed by chloroplast DNA: east-west lineage split and genetic mixture within western subtropical China. *PeerJ*, **7**: e6355.

Yang D, Liu XY. 2010. Fauna Sinica, Insecta, Megaloptera, Vol. 51. Beijing:

Science Press. (in Chinese)
Yang F, Chang WC, Hayashi F, et al. 2018. Evolutionary history of the complex polymorphic dobsonfly genus *Neoneuromus* (Megaloptera: Corydalidae). *Systematic Entomology*, **43**(3): 568–595.
Ye Z, Chen PP, Bu WJ. 2016. Terrestrial mountain islands and Pleistocene climate fluctuations as motors for speciation: a case study on the genus *Pseudovelia* (Hemiptera: Veliidae). *Scientific Reports*, **6**: 33625.
Ye Z, Yuan JJ, Li M, et al. 2018. Geological effects influence population genetic connectivity more than Pleistocene glaciations in the water strider *Metrocoris sichuanensis* (Insecta: Hemiptera: Gerridae). *Journal of Biogeography*, **45**(3): 690–701.
Ye Z, Yuan JJ, Zhen YH, et al. 2020. Local environmental selection and lineage admixture act as significant mechanisms in the adaptation of the widespread East Asian pond skater *Gerris latiabdominis* to heterogeneous landscapes. *Journal of Biogeography*, **47**(5): 1154–1165.
Ye Z, Zhu GP, Chen PP, et al. 2014. Molecular data and ecological niche modelling reveal the Pleistocene history of a semi-aquatic bug (*Microvelia douglasi douglasi*) in East Asia. *Molecular Ecology*, **23**(12): 3080–3096.
Yu HT. 1995. Patterns of diversification and genetic population structure of small mammals in Taiwan. *Biological Journal of the Linnean Society*, **55**(1): 69–89.
Yu Y, Harris AJ, Blair C, et al. 2015. RASP (reconstruct ancestral state in phylogenies): a tool for historical biogeography. *Molecular Phylogenetics and Evolution*, **87**: 46–49.
Zhang DL, Ye Z, Yamada K, et al. 2016. Pleistocene sea level fluctuation and host plant habitat requirement influenced the historical phylogeography of the invasive species *Amphiareus obscuriceps* (Hemiptera: Anthocoridae) in its native range. *BMC Evolutionary Biology*, **16**(1): 174.
Zhang RZ. 1999. Zoogeography of China. Beijing: Science Press. (in Chinese)
Zhang YM, Xie CF, Fu TA, et al. 2005. Tectonic evolution of Hainan Island. *Science Technology and Engineering*, **5**(20): 1485–1487. (in Chinese)
Zhao HT, Wang LR, Yuan JY. 2007. Origin and time of Qiongzhou Strait. *Marine Geology & Quaternary Geology*, **27**(2): 33–40.
Zhao WZ, Tan K, Zhou DY, et al. 2014. Phylogeographic analysis of *Apis cerana* populations on Hainan Island and southern mainland China, based on mitochondrial DNA sequences. *Apidologie*, **45**(1): 21–33.
Zheng YC, Dai Q, Guo XG, et al. 2020. Dynamics behind disjunct distribution, hotspot-edge refugia, and discordant RADseq/mtDNA variability: insights from the Emei mustache toad. *BMC Evolutionary Biology*, **20**(1): 111.
Zhu F, Liu Q, Che J, et al. 2016a. Molecular phylogeography of white-lipped tree viper (*Trimeresurus*; Viperidae). *Zoologica Scripta*, **45**(3): 252–262.
Zhu GP, Ye Z, Du J, et al. 2016b. Range wide molecular data and niche modeling revealed the Pleistocene history of a global invader (*Halyomorpha halys*). *Scientific Reports*, **6**: 23192.
Zhu H. 2016. Biogeographical evidences help revealing the origin of Hainan Island. *PLoS One*, **11**(4): e0151941.
Zhu H. 2017. Families and genera of seed plants in relation to biogeographical origin on Hainan Island. *Biodiversity Science*, **25**(8): 816–822. (in Chinese)